Title

Structure-specific amyloid precipitation in biofluids

M. Rodrigues[1,2], P. Bhattacharjee [3,4], A. Brinkmalm[3,4], D. T. Do[5], S. De[1,2], A. Ponjavic[1,6], J. A. Varela[1,7], S.F. Ruggeri[1], I Baudrexel[1], JE Lee[1,8], K Kulenkampff[1,2], TPJ Knowles[1], T. N. Snaddon[5], H. Zetterberg[3,4,9,10], S. Gandhi[9,11], S. F. Lee[1] and D. Klenerman[1,2,]

[1] *Department of Chemistry, University of Cambridge, Lensfield Road, Cambridge, CB2 1EW, UK*

[2] *UK Dementia Research Institute, University of Cambridge, Cambridge, CB2 0XY, UK.*

[3] *Department of Psychiatry and Neurochemistry, Institute of Neuroscience and Physiology, the Sahlgrenska Academy at the University of Gothenburg, S-431 80 Mölndal, Sweden*

[4] *Clinical Neurochemistry Laboratory, Sahlgrenska University Hospital, Mölndal, Sweden*

[5] *Department of Chemistry, Indiana University, 800 E. Kirkwood Ave. Bloomington, IN 47405, USA.*

[6] *School of Physics and Astronomy, University of Leeds, Leeds, UK*

[7] *Biomedical Sciences Building, University of St Andrews, North Haugh, St Andrews KY16 9ST, UK*

[8] *Department of Physics and Biology, University of York, Heslington York YO10 5DD, UK*

[9] *Department of Neurodegenerative Disease, UCL Institute of Neurology, London, WC1N 3BG, UK*

[10] *UK Dementia Research Institute at UCL, London, UK*

[11] *The Francis Crick Institute, 1 Midland Road, King's Cross, London, NW1 1AT, UK*

Abstract

The composition of soluble toxic protein aggregates formed in vivo is currently unknown in neurodegenerative diseases, due to their ultra-low concentration in human biofluids and their high degree of heterogeneity. Here we report a method to capture amyloid-containing aggregates in human biofluids in an unbiased way, a process we name amyloid precipitation. We use a structure-specific chemical dimer, a Y-shaped, bio-inspired small molecule with two capture groups, for amyloid precipitation to increase affinity. Our capture molecule for amyloid precipitation (CAP-1) consists of a derivative of Pittsburgh Compound B (dimer) to target the cross β-sheets of amyloids and a biotin moiety for surface immobilization. By coupling CAP-1 to magnetic beads, we demonstrate that we can target the amyloid structure of all protein aggregates present in human cerebrospinal fluid, isolate them for analysis and then characterize them using single-molecule fluorescence imaging and mass spectrometry. Amyloid precipitation enables unbiased determination of the molecular composition and structural features of the in vivo aggregates formed in neurodegenerative diseases.

Introduction

α-synuclein, amyloid-β and tau are examples of proteins that self-aggregate in cross β-sheets motifs, and are present in Lewy bodies, amyloid plaques, and tau tangles respectively[1]. These cross β–sheets or amyloid structures are found in the brains of people with neurodegenerative diseases such as Parkinson's and Alzheimer's[2] however, the exact mechanism by which protein aggregates lead to progressive loss of neuronal cells and subsequently pathophysiologic effects like dementia and movement disorders remains poorly understood. Test-tube studies, have revealed that protein aggregation is a dynamic process where a wide range of aggregates with variable sizes, and hydrophilicities[3] are formed and that the aggregates become more toxic when they convert to a β–sheets structure [4]. Previous studies have also shown that these small soluble protein aggregates (< 200 nm) are implicated in cellular toxicity[5–9], making the characterisation of these species a fundamental step toward the development of effective therapeutic targets. In the brain and biofluids, protein aggregates are present at very low (sub-picomolar) concentrations and they are very heterogeneous in size.[10,11]. Together these two factors have resulted in a lack of suitable tools to isolate and study protein aggregates. Until recently, proteins implicated in neurodegeneration have largely been characterised using capture based on antibodies or aptamers [12,13]. However, antibody or aptamer capture has intrinsic limitations such as epitope accessibility, which can lead to inefficient targeting of aggregates, depending on the extent of post-translational modifications, and targeting the range of aggregates, with different protein compositions and structures formed during the development of neurodegenerative disease.

To address these issues we have developed a "chemical antibody" designed to selectively bind protein aggregates associated with neurodegenerative disease which is based on the small molecules that have already been designed to target amyloid present in plaques[14]. This approach overcomes the limitations imposed by targeting a specific epitope on the protein by instead, specifically targeting β-sheets, a common structural feature in neurodegenerative diseases[11]. This is a non-biased approach to study the natural occurring small protein aggregates, involved in neurodegeneration. We have named this new molecule, capture molecule for amyloid precipitation, CAP-1. Protein aggregates can be precipitated out of from solution by attaching CAP-1 to magnetic beads, amyloid precipitation (AP). This AP approach enables an array of molecular and cellular techniques, from single molecule imaging to cytotoxicity studies to be performed to characterise the structural and functional properties of protein aggregates.

Materials and Methods

Synthesis of* N-biotinylated bis-benzothiazole: *CAP-1

Preparation of Linkers:

(A) bis-Mesylate:

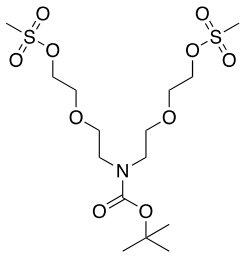

Triethylamine (2.53 mL, 18.0 mmol, 3.6 equiv.) was added dropwise to a solution of *diol* (1.47 g, 5.0 mmol, 1.0 equiv.) in dry CH_2Cl_2 (10 mL) at 0 °C. After stirring for 5 minutes a solution of methanesulfonyl chloride (1.01 mL, 13 mmol, 2.6 equiv.) in CH_2Cl_2 (5 mL) was added dropwise. Following complete addition, the cooling bath was removed, and the reaction was allowed to warm to rt and stirred for an additional 18 h. Thereafter, aqueous hydrochloric acid (1N, 100 mL) was added slowly with vigorous stirring. The reaction mixture was transferred to a separatory funnel and the aqueous layer was extracted with CH_2Cl_2 (4 × 60 mL). The combined organic layers were washed with sodium bicarbonate solution (50 mL) and brine (60 mL), dried over Na_2SO_4, filtered and concentrated under reduced pressure to give the bis-mesylate **(A)** (1.57 g, 3.5 mmol, 70%) as a colourless oil. IR (Film): 2974.06, 2939.12, 2874.49, 1693.46, 1681.7, 1545.05, 1479.45, 1455.55, 1415.74, 1392.37, 1246.98, 1172.02, 1068.5, 972.43, 920.11, 862.26 cm^{-1}. ^1H NMR (500 MHz, $CDCl_3$): δ = 4.33 (m, 4H), 3.7 (m, 4H), 3.59 (m, 4H), 3.44 (m, 4H), 3.03 (s, 6H), 1.43 (s, 12H). ^{13}C NMR (126 MHz, $CDCl_3$): δ = 155.34, 79.88, 69.86, 68.83, 47.70, 37.58, 28.40. HRMS (EI): m/z calcd for [M+Na] $C_{15}H_{31}NNaO_{10}S_2$ 472.1281. Found 472.1275

(B**)** Boc-protected bis-benzothiazole):

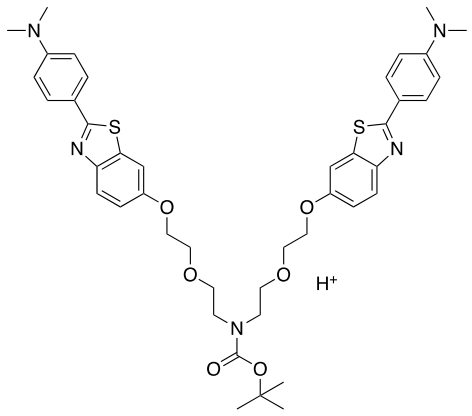

Sodium hydride (60% in oil, 19 mg, 0.44 mmol, 2.2 equiv) was added in one portion to a solution of the 2-(4-(dimethylamino)phenyl)benzo[*d*]thiazol-6-ol (110 mg, 0.4 mmol, 2.0 equiv) in DMF (5 mL). The resulting suspension was stirred for 1 h giving a colourless solution to which the bis-mesylate **A** (neat, 90 mg, 0.2 mmol, 1.0 equiv) was added dropwise via syringe. The resulting solution was heated to 80 °C for 18 h before being cooled to rt. H_2O (15 mL) was added with vigorous stirring and the resulting precipitate was collected by filtration, washed with water and Et_2O and dried over Na_2SO_4 to give the Boc-protected bis-benzothiazole **(B)** (64 mg 0.08 mmol, 40%) as white solid. Melting point: 122–124 °C. IR (Film): 2930.68, 1683.63, 1608.38, 1560.48, 1410.42, 1365.42, 1263.95, 1225.53, 1130.13, 1064.75, 1006.13, 967.19, 942.68, 863.88 cm^{-1}. ^1H NMR (500 MHz, $CDCl_3$): δ = 7.91–7.81 (m, 6H), 7.31 – 7.24 (m, 2H), 7.03 (dd, J = 8.9, 2.5 Hz, 2H), 6.69 (d, J = 8.6 Hz, 4H), 4.10 (d, J = 4.8 Hz, 2H), 3.84 – 3.76 (m, 4H), 3.72 – 3.62 (m, 4H),

3.56 – 3.44 (m, 4H), 3.01 (s, 12H), 1.45 (s, 9H). ^{13}C NMR (126 MHz, $CDCl_3$): δ = 166.56, 156.24, 155.48, 151.84, 149.05, 135.72, 128.47, 122.67, 121.56, 115.39, 111.68, 105.36, 79.64, 70.08, 69.49, 69.37, 68.06, 48.03, 47.78, 40.14, 28.45. HRMS (EI): m/z calcd for [M+H] $C_{43}H_{52}N_5O_6S_2$ 798.3354. Found 798.3383.

(C) NH bis-benzothiazole:

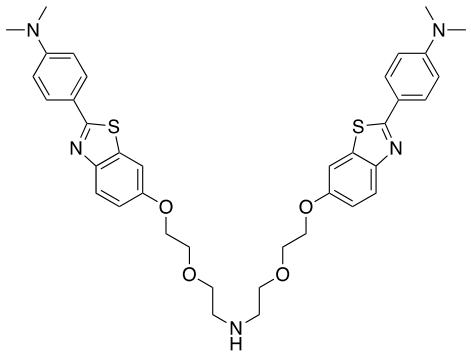

Boc-protected bis-benzothiazole (**B)** (64 mg 0.08 mmol) was added to a solution of HCl in MeOH (4M, 3 mL) and stirred for 1 h. The solution was quenched by careful addition of NaOH (3M, 10 mL) and EtOAc (10 mL) added. The layers were separated and the aqueous layer further extracted with EtOAc (2 × 10 mL). The combined organic extracts were dried over Na_2SO_4, filtered and concentrated to give the NH bis-benzothiazole **(C)** (55 mg, 80 mmol, 99%) as light yellow solid. Melting point: 168–170 °C. IR (Film): 3400.99, 2916.89, 1608.26, 1560.29, 1531.07, 1285.42, 1262.91, 1123.86, 1005.96, 966.67, 941.21, 818.48 cm^{-1}. ^{1}H NMR (400 MHz, $CDCl_3$): 7.86 (d, J = 8.6 Hz, 4H), 7.83 (d, J = 8.9 Hz, 2H), 7.27 (d, J = 2.5 Hz, 2H), 7.03 (dd, J = 8.9, 2.5 Hz, 2H), 6.70 (d, J = 8.6 Hz, 4H), 4.12 (t, J = 4.7 Hz, 4H), 3.82 (t, J = 4.7 Hz, 4H), 3.68 (t, J = 5.2 Hz, 4H), 3.02 (s, 12H), 2.88 (t, J = 5.2 Hz, 4H). ^{13}C NMR (126 MHz, $CDCl_3$): δ = 166.62, 156.23, 151.89, 149.10, 135.75, 128.52, 122.70, 121.62, 115.44, 111.72, 106.11, 106.08, 105.42, 70.51, 69.57, 68.04, 49.09, 40.17, 29.70. HRMS (EI): m/z calcd for [M+H] $C_{38}H_{44}N_5O_4S_2$ 698.2829. Found 698.2852.

(D) **N-Biotinylated bis-benzothiazole:**

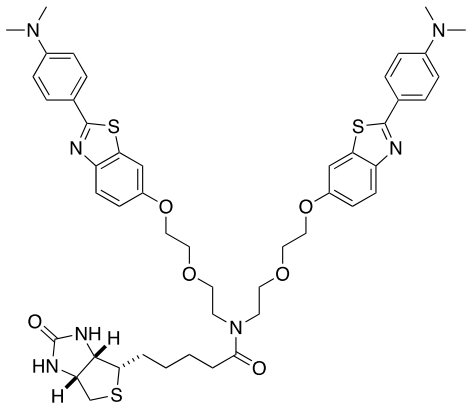

A solution of biotin (49 mg, 0.2 mmol, 1 equiv) in anhydrous DMF (2 mL) was freshly prepared and *i*Pr_2NEt (452 μL, 0.26 mmol, 1.3 equiv) and benzotriazol-1-yl-oxytripyrrolidinophosphonium hexafluorophhosphate (PyBOP, 135 mg, 0.26 mmol, 1.3 equiv) added sequentially. The resulting solution was stirred at rt for 30 minutes before a solution of the amine **C** (140 mg, 0.2 mmol, 1 equiv) and *i*Pr_2NEt (350 μL, 1.0 equiv) in DMF (1 mL) was added dropwise and the reaction stirred at rt for a further 18 h. Thereafter, sat. aq. NH_4Cl (10 mL) was added and the mixture extracted with EtOAc (3 × 5 mL). The combined organic layers were washed with brine (10 mL), dried over Na_2SO_4, filtered and concentrated under reduced pressure. The solid residue was purified by column chromatography [SiO_2, Methanol–CH_2Cl_2, 1:8] to **N-biotinylated**

bis-benzothiazole (CAP-1) (D) (56 mg, 0.06 mmol, 30%) as a light yellow solid. Melting point: 120–122 °C. IR (Film): 3257.07, 2929.35, 1698.51, 1606.39, 1560.35, 1533.11, 1490.89, 1365.68, 1264.49, 1210.08, 1125.77, 1066.65, 941.35, 819.84 cm^{-1}. ^{1}H NMR (400 MHz, $CDCl_3$): δ = 7.88 (d, J = 8.9 Hz, 4H), 7.85 (d, J = 8.9, 2H), 7.84 (d, J = 8.9, 2H), 7.31 (d, J = 2.5 Hz, 1H), 7.28 (d, J = 2.5 Hz, 1H), 7.04 (dd, J = 8.9, 2.5 Hz, 1H), 7.03 (dd, J = 8.9, 2.5 Hz, 1H), 6.73 (d, J = 8.9 Hz, 2H), 6.72 (d, J = 8.9 Hz, 2H), 5.24 (s, 1H), 4.65 (s, 1H), 4.40 – 4.28 (m, 1H), 4.14 (t, J = 4.6 Hz, 2H), 4.10 (t, J = 4.6 Hz, 3H), 3.82 (d, J = 4.6 Hz, 2H), 3.77 (dd, J = 5.5, 3.7 Hz, 2H), 3.72 (q, J = 3.1 Hz, 2H), 3.66 (d, J = 5.2 Hz, 2H), 3.62 – 3.56 (m, 5H), 3.16 (h, J = 3.5 Hz, 1H), 3.05 (s, 6H), 3.04 (s, 6H), 2.96 – 2.90 (m, 1H), 2.78 (dd, J = 12.8, 5.0 Hz, 1H), 2.66 – 2.59 (m, 1H), 2.52 (m, 1H), 2.36 (q, J = 7.1 Hz, 2H), 1.85 – 1.80 (m, 1H), 1.67 (m, 6H), 1.58 (q, J = 7.5 Hz, 3H), 1.31 (d, J = 16.4 Hz, 3H). ^{13}C NMR (126 MHz, $CDCl_3$) δ = 172.83, 170.48, 169.23, 165.99, 163.07, 156.59, 152.51, 149.07, 135.78, 128.56, 122.89, 121.20, 116.02, 112.37, 106.50, 79.63, 69.66, 69.39, 69.16, 68.55, 61.61, 59.83, 59.79, 55.85, 55.60, 48.55, 46.08, 40.24, 40.15, 32.54, 30.62, 28.76, 28.73, 28.56, 28.36, 28.03, 25.96, 25.73, 25.38, 24.78. HRMS (EI): m/z calcd for [M+H] $C_{48}H_{58}N_7O_6S_3$ 924.3605. Found 924.3618.

Aggregation of α-synuclein

Monomeric wild-type α-synuclein was purified from *Escherichia coli* as previously described [15]. Prior to use, α-synuclein aliquots were ultracentrifuged at 350000 *g* during 1h at 4 °C using TL120.2 rotor (Beckman) in a Optima TLX Ultracentrifuge (Beckman) to remove possible seed contaminants. 2/3 of the total volume in the tube was used as the supernatant fraction (monomers only) and removed with minimal perturbation to avoid remixing of unwanted seeds. Afterwards, the protein concentration was determined using a nanodrop ($\varepsilon^{275\ nm}$ (Tyr) 5600 $M^{-1}cm^{-1}$) and then the α-synuclein was diluted in cold Tris buffer 25 mM supplemented with 100 mM NaCl, pH 7.4 and 0.01% NaN_3 (to prevent bacterial growth) to a final concentration of 70 μM. This solution was incubated in the dark at 37°C with constant agitation at 200 rpm (New Brunswick Scientific Innova 43) and aliquots were taken at desired times (0h monomers, 6-8h oligomers and 1 – 5 d for mature fibrils). All time points were imaged on TIRFM setup before any experiment to confirm the presence/absence of the desired α-synuclein intermediate species *i.e* absence of aggregates at t0h and fibrils on 6-8h and presence of diffracted limited size aggregates on the 6-8h time point aliquots. All steps were carried out using LoBind microcentrifuge tubes (Eppendorf, Hamburg, Germany) to limit surface adsorption.

Preparation and photophysical characterization of CAP-1

CAP-1 1mM stock solution was prepared in DMSO, divided into 20 μL aliquots and stored a -20 °C. Aliquots were used once to avoid freeze and thaw cycles. The photophysical properties of CAP- 1 were determined using a Varian Cary Eclipse fluorescence spectrophotometer (Mulgrave, Australia). Experimental settings used were λ_{ex} = 355 nm (5 - 10 nm bandwidth), λ_{em} = 370-600 nm (5 - 10 nm bandwidth). UV–vis absorption and fluorescence (both excitation and emission) spectral characterization of CAP-1 (20 μM) were carried out in both PBS and Tris 25 mM supplemented with 100 mM NaCl, pH 7.4. For binding affinity experiments α-synuclein fibrils were sonicated on a probe sonicator (Bandelin, Sonopuls HD 20170), 4 times of 15 s at 10% power and the tube was placed on a beaker containing ice to minimise overheating effects on the tube walls.

Amyloid precipitation assay – AP

The amyloid precipitation (AP) assay consists of the pulldown of protein aggregates (e.g. α–synuclein) using streptavidin-Dynabeads (MyOne^{TM} Streptavidin C1, Invitrogen) conjugated with CAP-1. Briefly, 30 μL of beads/sample were removed from the vial, resuspended in 1 mL PBS and placed on a magnet for 2-3 minutes for separation and the supernatant discarded (this step was repeated three times). Afterwards, the beads were resuspended in 1 mL of CAP-1 30 μM and the tube placed in a revolver mixer for incubation at room temperature during 1h. Following, the tube was placed on the magnet for 2-3 minutes and the supernatant discarded. The beads were washed three times with PBS as before. Finally, the beads were resuspended in 500 μL solution containing α–synuclein 10 μM (monomers alone, or mixture of aggregates) and left in the revolver mix for 2h or overnight at 4°C. In the end, the tube was placed on the magnet for 2-3 minutes and 450 μL of supernatant were removed to a clean tube and labelled as ‘depleted’ fraction, both the depleted fraction and the ‘beads’ were kept at 4°C until use. All steps were carried out in LoBind microcentrifuge tubes (Eppendorf, Hamburg, Germany) to limit surface adsorption.

Detection of bead-bound α–synuclein

After amyloid precipitation (AP) both ‘beads’ (diluted 1:32 in PBS) and the ‘depleted’ fraction were added to a 96-well half-area plate with clear bottom (Corning 3881, Kennebuck ME, USA) for bulk fluorescence measurement. The plate was placed in a plate reader (CLARIOstar; BMG Labtech, Ortenberg, Germany) and Fluorescence intensity (bottom reading) was measured straight away at room temperature using the following settings: end-point mode, 440-10/480-10 nm excitation and emission wavelengths respectively; or spectrum mode, excitation at 355 nm and emission from 380-600 nm.

Atomic Force Microscopy

AFM was performed on freshly cleaved mica substrates. 10 μL aliquots of each diluted sample were deposited on the substrate at room temperature, incubated for 10 min, rinsed with 1 mL Milli Q water, and then dried under a gentle nitrogen flow. AFM maps were generated by means of a JPK nanowizard2 system (JPK Instruments, Germany) operating in tapping mode and equipped with a silicon tip (PPP-NCHR, 5 Nm^{-1}) with a nominal radius of <10 nm.

Preparation of slides for single molecule measurements

Borosilicate glass coverslips (VWR international, 20 × 20 mm, product number 631-0122) were cleaned using an argon plasma cleaner (PDC-002, Harrick Plasma) for 1 h to remove impurities and contaminants and create a hydrophilic surface. Frame-seal slide chambers (9 ×9 mm^2, Biorad, Hercules, CA, product number SLF-0601) were affixed to the glass, and 50 μL of poly-L-lysine (70000−150000 molecular weight, Sigma-Aldrich, product number P4707-50 ML) was added to the coverslip on the inside of the chamber and incubated for 30 minutes before being washed with filtered PBS buffer (Whatman Anatop 25 0.02 μm). Each batch of coverslips was tested for fluorescent artefacts (*i.e.* false positives) by imaging ThT 5 μM. ThT stock solution was prepared as described elsewhere[16] and ThT working solution (50-100 μM) was filtered (Whatman Anatop 25 0.02 μm) prior to use and concentration determined using $\varepsilon^{412\ nm}$ 36000 $M^{-1}cm^{-1}$.

Total internal reflection fluorescence microscopy (TIRFM) imaging

Imaging was performed using a homebuilt total internal reflection fluorescence microscope as reported previously [16]. Briefly, this imaging mode restricts detectable axial fluorescence signal to within ~200 nm from the glass-water interface. For imaging of recombinant α-synuclein or CSF in the presence of ThT or CAP-1, the output from laser operating at 405 nm (Oxxius LaserBoxx, product number LBX-405-100-CIR-PP) was aligned and directed parallel to the optical axis at the edge of a 60x Plan Apo TIRF, NA 1.45 oil objective, (Nikon Corporation), mounted an Eclipse TE2000-U microscope (Nikon Corporation) fitted with a Perfect Focus unit. Fluorescence was collected by the same objective and was separated from the returning TIR beam by a dichroic (Di01-R405/488/561/635, Semrock), and passed through appropriate filter (FF01-480/40-25 or FF01-434/17-25 Semrock, for ThT or CAP-1, respectively). The images were recorded on an EMCCD camera (Evolve 512, Photometrics) operating in frame transfer mode (EMGain of 6.5 (or11.5) e−/ADU and 250 ADU/photon). Each pixel was 241 nm in size. For each data set, 4×4 image grids were measured in at least three different regions of the coverslip. The distance between the nine images measured in each grid was set to 350 μm, and was automated (bean-shell script, Micromanager) to prevent user bias. Images were recorded at 50 ms exposure time for 100 frames with 405 nm illumination (150–200 W/ c2).

Recombinant α-synuclein and CSF were diluted in filtered PBS (Whatman Anatop 25 0.02 μm) and mixed with ThT or CAP-1 for a final imaging volume of 50 μL. The ThT and CAP-1 imaging concentration was 5 μM while the α-synuclein concentration changed between experiments (1 μM for sonicated fibrils, 2.8 μM for comparison of time points, and 7 μM for t=8h). For CSF samples, we used 15 μL of neat CSF and 24 μL of depleted fraction AP. All samples were stored and diluted in LoBind microcentrifuge (Eppendorf, Hamburg, Germany) to limit surface adsorption. For imaging the beads (Figure 2 c) we used 1 μL of 'beads' fraction (50 μL in total) in 49 μL of PBS.

Imaging of amyloid-β_{1-42} and tau fibrils

1 μM amyloid-β_{1-42} ($a\beta_{42}$) and 100 nM tau fibrils were imaged in similar way to α-synuclein. Prior to imagining protein aggregates were diluted in PBS and incubated with either 5 μM of ThT or CAP-1, or 50 nM of pFTAA (tau). $A\beta_{42}$ fibrils were obtained by incubating 4 μM of monomeric amyloid-β_{1-42} (Stratech, Catalogue Number: A-1167-2-RPE) in PBS for 4h at 37°C with constant agitation. Tau aggregation reactions were performed using 50 μM 0N4R htau (InVivo BioTech Services GmbH, Germany) in buffer containing 100 mM Tris, 150 mM NaCl and 0.1 mM EDTA. The aggregation was initiated by the addition of 0.05 mg/ml heparin (1:4 heparin:tau ratio). The aggregation reaction was incubated at 37°C under quiescent conditions for 120 hours before imaging.

AP of α-synuclein spiked in CSF followed by on-bead digestion

The CSF sample aliquots used were de-identified leftover aliquots from clinical routine analyses, following a procedure approved by the Ethics Committee at University of Gothenburg (EPN 140811). Amyloid precipitation was carried out as described above, except for using 50 μL of beads per sample instead of 30 μL. After conjugation with CAP-1 and washing the beads were resuspended in a solution containing 600 μL of CSF and 400 μL PBS. α-Syn was spiked into the CSF, adding either monomer alone or a mixture containing monomers and oligomers (previously characterized using TIRFM). Concentrations spiked were 1 pM, 100 pM, 1 nM, 10 nM and 100 nM and samples were prepared in triplicate. The immunoprecipitation method for CSF samples was performed according to Bhattacharjee *et al.* 2019 with minor modifications[17,18]. Briefly, after overnight incubation at 4 °C the magnetic particle processor KingFisher (Thermo Fisher Scientific) was used to wash and resuspend the beads. The beads were first extracted, then washed two times with PBS, one time with 1 mL of 50 mM ammonium bicarbonate (NH_4HCO_3, pH 8.0; Sigma-Aldrich) and finally resuspended in 100 μL of 50 mM NH_4HCO_3 for on-bead digestion. For on-bead digestion 10 μl of 10 mM 1,4-dithiothreitol (DTT) in NH_4HCO_3 was added to the solution, vortexed and

incubated for 30 minutes at 60 °C and, then cooled down to room temperature for 15 min. Afterwards, 10 µl of 10 mM iodoacetamide (IAM) in NH_4HCO_3 was added, vortexed and incubated for 30 minutes at 25°C in darkness. Finally, 10 µl of trypsin 5 ng/µl in NH_4HCO_3 was added, vortexed and incubated at 37ºC overnight with shaking at 400 rpm. The reaction was stopped by addition of 10 µl 10% FA. Finally, samples were centrifuged at 16910 *g* for 10 min, 4°C and the supernatant collected in a different vial. The magnetic beads were washed with 50 µl NH_4HCO_3, then centrifuged again and the supernatant was collected in the same vial as before. Then collected supernatants were dried by speedvac.

LC-MS/MS of α-synuclein

High-resolution parallel reaction monitoring (PRM) analyses were performed on a quadrupole–orbitrap mass spectrometer Q-Exactive (Thermo Fisher Scientific) coupled to an Ultimate 3000 chromatography system (Thermo Fisher Scientific). Mobile phases were 0.1% aqueous FA(v/v) (A) and 0.1% FA in 84% ACN in water (v/v) (B). The mixture of Heavy-isotope-labeled peptide standards of α-synuclein (Heavy Peptide FasTrack 1 standards, ThermoFisher Scientific, USA) was prepared in 20% ACN containing 0.1% FA as follows: $\alpha\text{-syn}_{13\text{-}21}$, $\alpha\text{-syn}_{35\text{-}43}$, $\alpha\text{-syn}_{46\text{-}58}$, $\alpha\text{-syn}_{61\text{-}80}$, and $\alpha\text{-syn}_{81\text{-}96}$ (10 fmoles/µL each). Then the dried samples after pull down and on-bead digestion were dissolved in 20 µl of mixture of heavy-isotope-labelled (IS) peptide standards for 1 h and then transferred to LC vials for analysis. Samples were loaded directly onto a HypersilGold-C18 column, (length 100 mm, inner diameter 2 mm, particle size 1.9 µm, Thermo Fischer Scientific) with 0.1% aqueous FA at 300 µL/min. After 2 minutes of loading, the peptides were eluted off the column using the following linear gradient steps: 0 minutes 0%B; 4 minutes 17%B; 16 minutes 35%B; 17.5 minutes 100%B; 20 minutes 0%B. The global MS parameters were: positive ion mode; spray voltage 3.5 kV; vaporizer temperature +350°C; sheath gas pressure 40 psi; auxiliary gas pressure 25 arbitrary units; capillary temperature +350°C; collision gas pressure 1.9 mTorr. The instrument was set to acquire scheduled pairs or triplets of PRM scans and subsequent all ion fragmentation scans allowing simultaneous detection of both the α-synuclein peptide and the corresponding IS peptide standards. The settings were common for both scans types and were as follows: resolution, 70,000; AGC target, 3e6; maximum injection time, 250 ms; isolation window, 3.0 m/z and normalized collision energy 35. Data acquisition and analysis were performed with Xcalibur software version 2.2 SP1.48 (ThermoFisher Scientific) and Pinpoint 1.3.0 (ThermoFisher Scientific) for determining selected fragment ion peak areas, respectively. The MS accuracy was ± 10 ppm centred at 0, a MS/MS accuracy of ± 15 ppm and the isolation mode set to MS/MS with an isolation width of 3.0 u. The peaks were detected using a chromatographic peak with a window size of ± 2.0 min. The complete peak area was determined after using four points of smoothing. The scheduling

window size for identified transitions was ± 0.5 min. The detected fragment ion peaks were manually inspected for accuracy and absence of interferences from other peptides than the peptide of interest, including fragments originating from other product ions in the same pair/triplet. The relative amount of spiked unlabelled or 15N-labeled α-synuclein peptide was calculated by normalizing the measured peak area with the peak area of the corresponding IS peptide.

Database search parameters

Specified search parameters were database (Swissprot), taxonomy (Homo sapiens), enzyme (trypsin, Glu-C, Asp-N, trypsin + Glu-C or trypsin + GluC + Asp-N), variable modifications (acetyl [N-term] and oxidation [M]), static modification (carbamidomethyl [C]), mass values (monoisotopic), peptide mass tolerance (± 10 ppm), fragment mass tolerance (± 10 mmu), and maximum 2 missed cleavages. On average, individual ions scores > 40 indicate identity or extensive homology ($P < 0.05$) was considered for identification. Ions score is $-10\log(P)$, where P is the probability that the observed match is a random event.

Membrane permeability assay

Details of this method have been described previously[19]. Studies have shown that single vesicle assay can be used to measure the toxicity of β-sheet rich protein aggregates present in CSF[20] or complex biological mixture[8].Briefly, Phospholipids 16:0-18:1 1-palmitoyl-2-oleoyl-glycero-3-phosphocholinePC (Avanti Polar Lipids) and biotinylated lipids 1-oleoyl-2-[12-biotinyl(aminododecanoyl)]-sn-glycero-3-phosphocholine18:1-12:0 Biotin PC (Avanti Polar Lipids) were mixed 100:1 ratio and dissolved in HEPES buffer (pH 6.5) with 100 μM Cal-520. Using dry ice and a water bath, five freeze-and-thaw cycles were performed to control the unilamellarity. Then the mixed lipid solution was passed 10 times through an extruder (Avanti Polar Lipids, A) with a membrane of 200 nm diameter. To remove the free dye from the surrounding solution containing dye-filled vesicles, size-exclusion chromatography was performed using Superdex 200. The size of the vesicles was confirmed using a zeta-sizer. The vesicles are immobilised using biotin-neutravidin linkage in glass coverslips. Before immobilisation of the vesicles, each coverslip is cleaned using argon based plasma cleaner and sample chambers were made by affixing Frame-Seal incubation chambers onto the glass slides. For homogeneous surface treatment, 50 μL of a mixture of 100:1 PLL-g-PEG and PLL-g-PEG biotin (both 1 g/L) in HEPES buffer (50 mM, pH 6.5) was added to the coverslip inside of the chamber and incubated for 30 min. Then the surface was washed with filtered HEPES buffer and a solution of NeutrAvidin (50 μL of 0.1 mg/mL in MilliQ) added and incubated for 15 minutes before being washed. 50 μL of vesicles was added to the coverslip and let to adsorb for 20 minutes before solution is removed and replaced

by 30 μL of Ca^{2+} containing buffer solution Leibovitz's L-15 and background image was recorded ($F_{background}$). Thereafter, 16 μL of sample (16 μL of AP depleted fraction or 10 μL of neat CSF + 6 μL PBS) was added and incubated for 20 minutes and images were acquired (F_{sample}). Next, 10 μL of ionomycin solution added and same fields of view were acquired ($F_{ionomycin}$). For each field of view (10 to 15 in total) 50 images were taken with an exposure time of 50 ms. The relative Ca^{2+} influx into an individual vesicle due to protein aggregates present in CSF was then determined as

$$Ca^{2+}influx = \frac{F_{sample} - F_{background}}{F_{Ionomycin} - F_{background}}$$

The average degree of was calculated by averaging the Ca^{2+} influx into individual vesicles. The membrane permeabilization experiments were performed using a homebuilt TIRF imaging setup microscope using 1.49 100X Nikon TIRF Objective. For excitation 488-nm laser (Toptica) beam and images were acquired using an air-cooled EMCCD camera (Evolve Delta).

Electron microscopy

Electron microscopy images were acquired on a scanning electron microscopy with a retractable STEM detector (TESCAN MIRA3 FEG-SEM) using 30kv. Holey carbon grids (EM Resolutions, 300 mesh Copper) were glow-discharged for hydrophilization using Quorum Technologies GloQube Dual Chamber Glow Discharge System (25 mA, 60 sec, negative) and then 10 μL of α–synuclein samples (fibrils or sonicated fibrils) was added and let dry for 15 minutes (excess carefully removed with filter paper). Prior to imaging grids were plasma cleaned (Fischione Model 1070 Nanoclean Plasma Cleaner) using a 25% oxygen and 75% argon gas mixture to remove carbonaceous debris, for 15 sec.

Data analysis

Microscopy images were analysed using ImageJ and Matlab. GraphPad Prism 8 was used for statistical analysis, plotting and curve fitting. Statistical analysis was performed using unpaired two-tailed Student's t test to analyse differences between two groups, or a one-way ANOVA and Tukey's *post hoc* comparison to analyse differences among three or more groups. Differences were considered to be statistically significant if $p < 0.05$. To determine the number of fluorescent puncta in each image an average of the entire stack was generated and used to detect each protein aggregate using the Find Maxima function in ImageJ (with a threshold value of 180 Figure 2.e).

Results

Rational design and characterization of a bio-inspired amyloid-specific probe

The design of CAP-1 was inspired by the structure of antibodies due to their natural high affinity to target specific molecules, based on their Y shaped structure with two binding sites. This 'chemical antibody' contains structural elements of thioflavin T for its photophysical and optical properties [14,21] and structural elements of Pittsburgh compound B for its increased affinity to β-sheet structures compared with ThT[22,23] ,namely the aniline and tertiary benzothiazole group respectively.

The synthesis of CAP-1 was achieved using established methods; see Fig. 1a for structure and SI.1-5 for synthesis details. The trimeric species has two β-sheet binding sites for increased avidity (as previously described for a dimeric version of ThT[24]) and has a third site for immobilisation, in this specific implementation *via* biotin – streptavidin binding. After initial spectral characterisation of CAP-1, $\lambda_{ex\text{-}em}$ 355- 440 nm (SI.6) we evaluated the binding of CAP-1 to α-synuclein monomers, oligomers and fibrils. CAP-1 binds to oligomers and fibrils but not monomers, see Fig.1b-d and SI.8. CAP-1 like ThT[16] is suitable to total internal reflection fluorescence microscopy (TIRFM), and can be used to monitor the aggregation reaction, from small early stage aggregates (t > 4h) to long mature fibrils (t > 24h) (Fig.1c). The progressive increase in fluorescence intensity (Fig. 1d and SI.8) with increased incubation measured by bulk fluorescence further demonstrates CAP-1 specificity towards cross β-sheets. α-synuclein was selected as the model amyloid protein throughout this work but we also achieved similar results using other amyloid proteins such as $a\beta_{42}$ and tau aggregates (SI.9). The binding of CAP-1 to these protein aggregates further supports the specificity towards cross β-sheet regardless of protein sequence, highlighting the value of targeting a 'structural epitope' using CAP-1 to study aggregates in a non-biased way.

Finally, we determined the binding affinity of CAP-1 to α-synuclein and compared this affinity with that of ThT using bulk fluorescence and mature sonicated fibrils (average length 200 nm), to avoid heterogeneity in the structure and size of the aggregates, see SI.10. Using an initial concentration of 100 nM α-synuclein we obtained a K_d (CAP-1) = 82.63 ± 11.70 nM and K_d (ThT) = 3962 ± 352 nM (Fig.1e), a 50-fold increase in affinity of CAP-1 compared to ThT. Dissociation constants values often depends on the approach used and previous studies reported K_d of ThT for α-synuclein fibrils from 588 nM to 100 μM[25,26]. In a study using a similar methodology to ours but using $a\beta_{40}$ fibrils instead of α-synuclein the K_d was 2.3 μM[24]. The significant increase in CAP-1 affinity towards amyloids compared to ThT can be explained by the combination of two key factors: CAP-1 being a

dimer, as previously described avidity increases affinity[24] and the absence of the methylated nitrogen in benzothiazole group (SI.1) as seen for PiB[22,23].

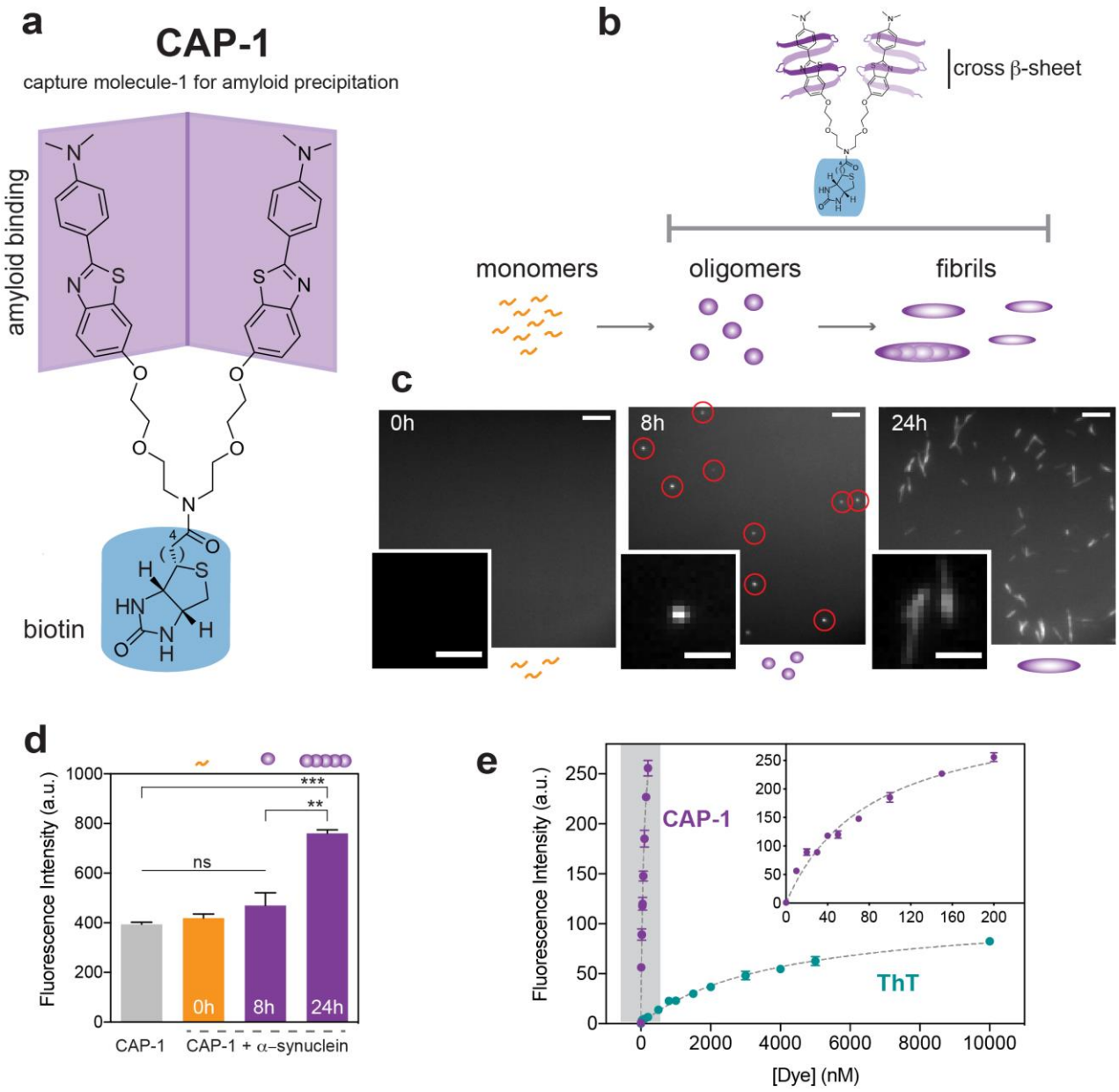

Figure 1 – Design and characterization of a bio-inspired amyloid-specific probe. (**a)** CAP-1 chemical structure. In purple the amyloid binding regions and in blue, biotin used for surface attachment *via* streptavidin binding. (**b**) Illustrative diagram highlighting the selective affinity of CAP-1 to cross β-sheets present in early stage aggregates and fibrils but not in monomers. (**c**) TIRFM images of α-synuclein aggregation at 0h, 8h (red circles highlighting oligomers) and 24h using 5 µM CAP-1, λ_{ex}405 nm. Scale bar = 5 µm, inset scale bar = 2 µm. (**d**) Fluorescence intensity increase of CAP-1 (20 µM) upon binding to 10 µM α-synuclein at different time points of the aggregation reaction using λ_{ex}355 nm. The error bar represents the SD of the maximum fluorescence intensity between two independent experiments. The *p*-value corresponds to the result of a one-way ANOVA, and Tukey's post hoc comparison. **p<0.0017, ***p=0.0007, n.s. p>0.05. (**e**) Binding affinity of CAP-1 and ThT to α-synuclein. Increasing amounts of CAP-1 or ThT were added to 100 nM α-synuclein. The K_d was obtained by fitting the experimental points to a hyperbolic curve (specific binding), K_d (CAP-1) = 82.63 ± 11.70 and K_d (ThT) = 3962 ± 352 nM.

Capture of protein aggregates using CAP-1 – Method of amyloid-precipitation

Following the characterization of CAP-1 binding to α–synuclein, we designed a protocol for isolation of protein aggregates from solution, which we have named amyloid-precipitation (AP). The schematic of AP is outlined in Fig. 2a-b. After the conjugation of CAP-1 with magnetic streptavidin-coated beads (Fig. 2a) the beads are added to a solution containing protein aggregates such as recombinant α–synuclein solution or a biofluid. After 2h at 4°C with gentle mixing, the beads are separated using a magnet and both fractions ('beads' and 'depleted') are analysed by TIRFM (Fig. 2c) and bulk fluorescence (Fig. 2d).

Fig. 2c shows conjugated beads with CAP-1 after AP using α–synuclein fibrils (right) or PBS (left). The presence of fibrils (right panel) attached to the beads is visible by the 'barbed' appearance of the beads and highlighted in the magnified bead, and contrasts with the plain look of beads without protein (left panel). Despite the heterogeneous bead-to-fibril attachment, some beads contain many small fibrils and others fewer but longer fibrils , there is a significant difference in the diameter (measured as fluorescence intensity profile) between beads in the presence or absence of α–synuclein fibrils, 105 nm (p = 0.0002) confirming the successful binding of fibrils to beads (see SI.11). In Fig. 2d we tested the efficacy of AP towards α–synuclein fibrils *versus* α–synuclein monomers (see SI.12 for representative fluorescent spectra of both fractions). The increase in fluorescence between the 'depleted' (11%) and 'beads' (100%) fraction for the beads+CAP-1+α–synuclein fibrils sample demonstrates the successful pulldown (and concentration) of aggregates by the beads. The difference between the beads+CAP-1+α–synuclein fibrils (purple - 100%) and beads+CAP-1+α–synuclein monomer (orange - 33%) highlights the absence of cross β-sheet in the monomeric solution as seen Fig.1 d. The 33% (orange) correspond to the fluorescence of CAP-1 alone. The low fluorescence intensity detected for the 'depleted' fraction of both samples, 11% for fibrils and 3% for monomers, respectively, reflects the presence of residual CAP-1 molecules released from the beads during the incubation and as expected is higher for the sample containing fibrils. The fluorescence of beads+CAP-1+monomers is the same as CAP-1 beads+CAP-1+PBS, for both 'beads' and 'depleted' fraction confirming that CAP-1 does not bind to monomers (see SI.12). In both TIRFM (Fig. 2c) and bulk (Fig. 2c) measurements, detection of protein aggregates is based on CAP-1 intrinsic fluorescence, highlighting its ability to strongly bind (capture) aggregates and work as optical readout for the presence of β-sheets.

We also used atomic force microscopy (AFM), an orthogonal non optical technique, to confirm the successful binding of α–synuclein fibrils to CAP-1-beads (SI.13). As shown in the 3D (height)

image fibrils localize preferentially close to the beads (SI.13a), once more demonstrating the preference of protein aggregates to CAP-1 coated beads.

So far, we have used mature α–synuclein fibrils (sonicated 200 nm, non-sonicated >1 μm) as a model of protein aggregation to test AP. However, in a biological fluids such as cerebrospinal fluid (CSF) the amyloids present are smaller, these 'early stage' aggregates, or oligomers, have been shown to be much smaller that the optical diffraction limit (~250nm)[16] and confirmed to be approximately 10s of nanometres in size using higher resolution methods such as AD-PAINT and AFM[27]. For this reason we used α–synuclein aggregates collected at the 8 hour time point to maximize the number of oligomers[4,3] and to validate the AP method for use in a biological context. We used EM to characterize aggregates present at 8h (SI.16) and confirmed their sub diffraction limit size (~30 nm). The results in Fig. 2e show the number of fluorescent puncta before and after amyloid precipitation, 6.0 $x10^{-2}/\mu m^2$ and 3.6 $x10^{-4}/\mu m^2$, respectively (see SI.15 TIRFM images). In the presence of CAP-1 the number of protein aggregates in solution after pulldown is reduced to background levels (Fig. 2e, grey column - 4.2 $x10^{-4}$ ± 2.3 $x10^{-4}$ $/\mu m^2$). In the absence of CAP-1 there was partial removal of aggregates (see SI.15) suggesting unspecific binding to the beads but negligible compared to the virtually complete depletion, 99.4%, in the presence of CAP-1.

Next we investigated the use of mass spectrometry (MS) to quantify the amount of α–synuclein enriched on the beads after pulldown as MS will allow identification of molecular composition of the amyloids captured using AP. For this, we used high-resolution parallel reaction monitoring (PRM) mass spectrometry (MS). After AP, the beads were separated and digested using trypsin, converting full length α-synuclein into small peptides, namely α-syn_{13-21}, α-syn_{35-43}, α-syn_{46-58}, α-syn_{61-80}, and α-syn_{81-96}, see Fig. 2. The PRM-MS spectrum in Fig. 2g shows the relative abundance of each peptide. In order to confirm the specificity of CAP-1, we compared the presence and absence of CAP-1 during the AP. In the presence of CAP-1 the amount of individual peptides was 5 to 13 times higher, depending on the peptide, than without CAP-1 (Fig. SI.17). This is in agreement with TIRFM results (Fig. 2e).

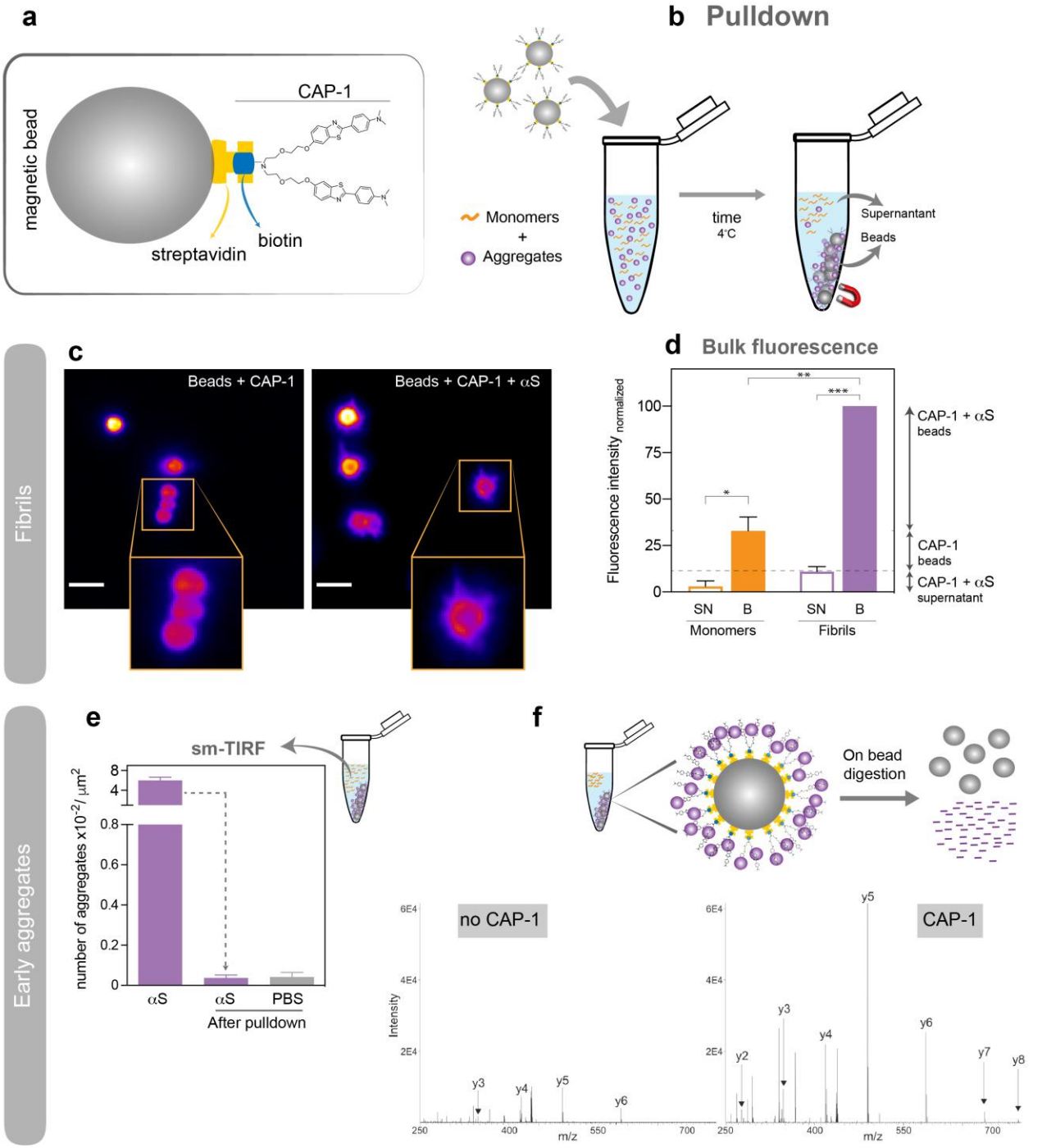

Figure 2 – Amyloid-precipitation using CAP-1. (**a**) Magnetic Dynabeads coated with streptavidin conjugated with CAP-1 via biotin moiety. (**b**) Outline of the amyloid-precipitation (AP) method. Functionalised beads with CAP-1 are incubated with an amyloid containing solution. After incubation beads bound to proteins aggregates are isolated using a magnet. Both fractions, depleted (supernatant) and enriched fraction (beads) can be analysed by bulk fluorescence and TIRFM. (**c**) TIRFM of Dynabeads Streptavidin C1 coated with CAP-1 and in the presence (right panel) or absence (left panel) of 10 µM α-synuclein fibrils (right panel) using λ_{ex} 405 nm. α-synuclein fibrils can be seen attached to the beads creating a 'hairy' bead look (right panel detail) or in other cases as a single long and thick spike. In the absence of protein aggregates (left panel) beads have a plain look. Scale bar = 3 µm. (**d**) Bulk fluorescence intensity (normalised) of beads and supernatant after AP using 10 µM α-synuclein, (■) 100 % of monomers and (■) sonicated fibrils (5 days incubation), λ_{ex} 355 nm and λ_{em_max}. The error bar represents the SD of the maximum fluorescence intensity between two independent experiments (each made in triplicate) and differences between two groups were analysed using

unpaired two-tailed Student's t test, *p=0.0345, **p=0.0062 and ***p=0.0004. (**e**) Depletion of α-synuclein oligomers (time point 8h of α-synuclein aggregation reaction) by AP and quantification of aggregates left in the supernatant (depleted fraction). Plotted is the fluorescent puncta counts $x10^2/\mu m^2$ for the sample before and after AP using TIRFM. AP captures approximately ~100% of oligomers in solution. The error bar represents the SD of the number of fluorescence puncta between at least 27 fields of view for one representative experiment (see SI.15 for TIRFM images) (**f**) Outline of AP followed by on bead digestion. $\alpha\text{-synuclein}_{13\text{-}21}$ peptide fragment ion PRM spectrum in the presence (right) and absence (left) of CAP-1, recovered after AP from a solution containing 1 nM total α-synuclein (<50 pM oligomers). (right).

Amyloid-precipitation followed by PRM mass spectrometry of α-synuclein spiked in human CSF

AP is an unbiased method to capture amyloid protein from solution but also a method that allows subsequent mass spectrometry identification of proteins present in such aggregates[28,29]. As CSF is a complex biofluid made of more than two thousand different proteins [30], we firstly determined the sensitivity of CAP-1-beads to capture known amounts of α–synuclein spiked in CSF. Increasing amounts of either purified α–synuclein monomers (t = 0 hours) or α–synuclein mixture of monomers (>95%) and oligomers (<5%)[4] (t = 8 hours), were spiked in control CSF, see Fig. 3a for the outline of the experiment and SI.18 for TIRFM representative images. After AP, beads were trypsin-digested and analysed by PRM-MS. In Fig. 3b the amount of α–synuclein$_{13\text{-}21}$ peptide recovered as a function of the initial α–synuclein concentration spiked is shown. Naturally occurring α–synuclein oligomers present in CSF were undetectable. For concentrations equal to and below 1 nM, monomers were not detected, while in 1 nM of mixed species 28 femtomoles (28 pM) of α–syn$_{13\text{-}21}$ captured were detected (SI.17 for other peptides). For α–synuclein concentrations higher than 1 nM, the increase in α–syn$_{13\text{-}21}$ detected is linear and about three times higher for the mixed species sample than for the monomers. This difference is amplified if we take into account that the only difference between samples is that there is present <5% of aggregated α–synuclein in the mixed sample. CAP-1-beads captured only 0.6 % of total monomers spiked in CSF but 2.34 % in the case of the aggregated sample. This means that almost no monomers in solution are captured while approximately 50 % (2.34% out of <5%) of the oligomers added to CSF are captured. These results confirm the specificity of AP in capturing protein aggregates compared to the monomers in complex biofluids such as CSF.

To evaluate the efficiency of AP in removing toxic amyloid species from CSF we used a sensitive membrane permeability assay previously developed [19] (see Fig. 3c for outline of the experiment). CSF is diluted in a solution containing Ca^{2+} and then added to liposomes containing a Ca^{2+}-dependent dye encapsulated. If CSF contains amyloids/oligomers that cause causes membrane permeability, Ca^{2+} enters the liposome resulting in increased fluorescence. In Fig. 3d, the average Ca^{2+} influxes for CSF before AP (purple), CSF after AP ('depleted' fraction) (white) and CSF after AP without CAP-1 (white with purple dots) using the same CSF as in Fig. 3b it is plotted. AP removed most of the CSF proteins responsible for Ca^{2+} influx, reducing membrane permeability from 27% to 6%. It is worth noting that there is non-specific binding to the beads without CAP-1 that leads to some aggregate capture and a small reduction in membrane permeability. Having established that AP is able to remove amyloid proteins from control CSF (Fig. 3b-d), we then

decided to use CSF from Parkinson's disease (PD) patients in a separate set of experiments (Fig. 3e-f). TIRFM images showed a significant decrease in the number of ThT active species after AP Fig. 3g (left panels) and we found that there was a reduction of ~50% in Ca^{2+} influx. This demonstrates that AP can capture amyloid aggregates from PD CSF. The difference between the results for control and PD CSF suggest that there are an increased number of non-amyloid aggregates present in the PD CSF that can also permeabilise the membrane but are not captured using CAP-1.

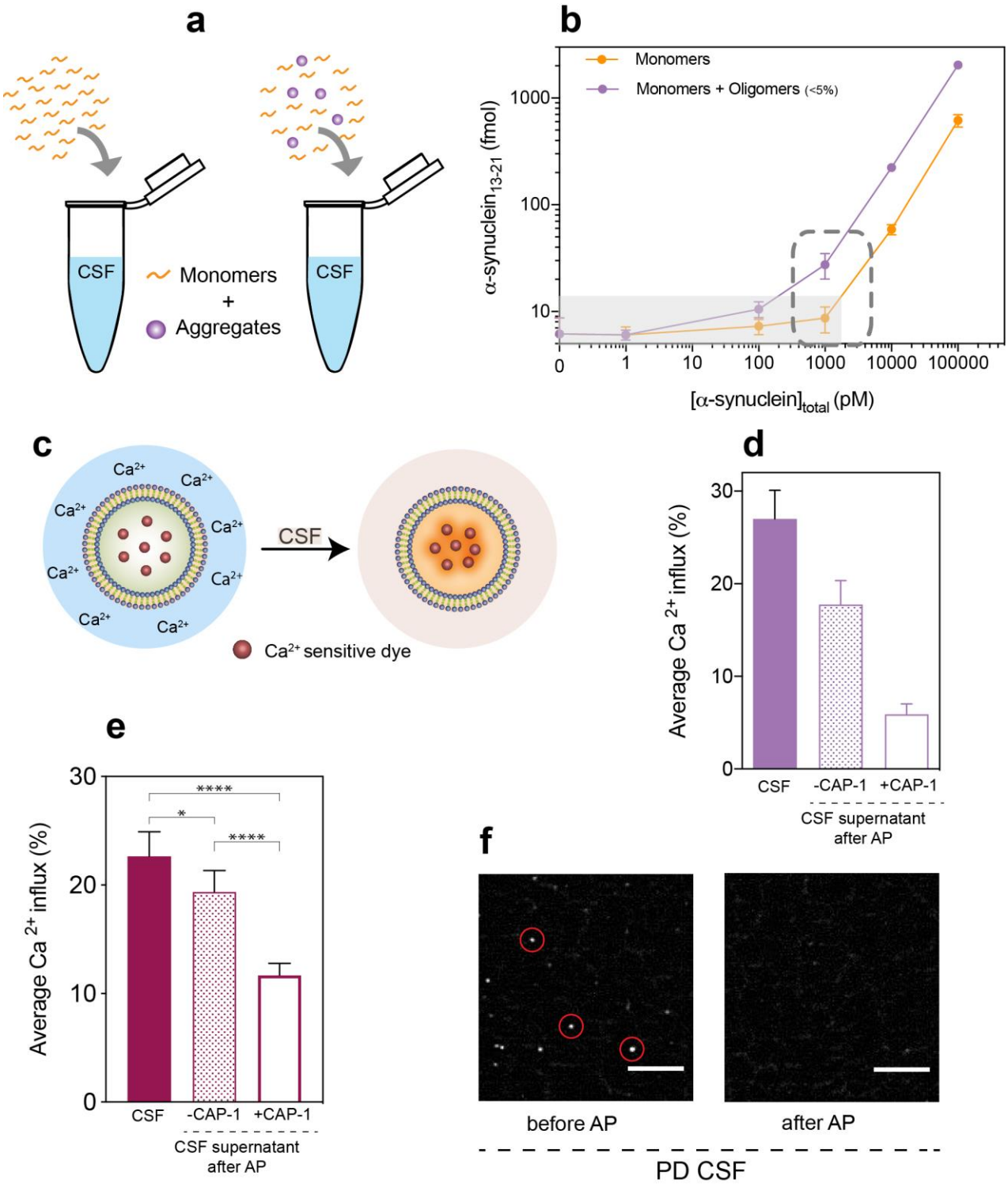

Figure 3 – Amyloid-precipitation of CSF spiked with recombinant α-synuclein oligomers. (**a**) Outline of the experiment. Known amounts of recombinant α-synuclein monomers or mixture of oligomers + monomers (<95%) are spiked into control CSF. (**b**) Quantification of α-synuclein$_{13\text{-}21}$ peptide recovered from on-bead digestion after AP using PRM-MS. Results were plotted as amount of α-synuclein$_{13\text{-}21}$ peptide recovered in fmol as a function of the initial α-synuclein concentration used for AP in pM. from α-synuclein monomers (-•-) and from α-synuclein mixture (oligomers+monomers) (-•-). (**c**) Outline of the membrane permeabilization essay. (**d**) Average Ca^{2+} influx in control CSF (used in **b**) before and after AP, and after AP in the absence of CAP-1. Mean and SD for the average Ca^{2+} influx for at least 10 to 15 fields of view for one representative experiment. (**e**) Average Ca^{2+} influx of PD CSF sample before and after AP in the presence of CAP-1 and, after AP in the absence of CAP-1. Mean and SD for the average Ca^{2+} influx

between five independent patients (10 to 15 fields of view used for each patient) and *p*-value from a one-way ANOVA, and Tukey's post hoc comparison. ***p<0.001, *p=0.0255. (**f**) Example of TIRFM image of PD CSF sample before (left) and after (right) AP, λ_{ex}405 nm and 5 μM ThT.

Discussion

Protein aggregates have been known to be implicated in neurodegenerative diseases for more than three decades[31]. Yet, despite much progress there are still significant technological limitations in isolating and characterising the intermediate small species that are formed during the development of disease. Traditional immunocapture/immune recognition approaches face challenges of sequence specificity, epitope accessibility and post-translational modifications. In contrast, "chemical antibodies" can target the amyloid structure, which is present in toxic and pathological aggregates, independent of its protein composition. In this study, we presented the synthesis and characterisation of an aggregate specific 'chemical antibody' designed to capture protein aggregates associated with neurodegeneration from solution. This molecule has been specifically developed to bind and isolate a target molecule based on secondary structure. Previous studies have made use of dimerised ligands (protein/peptide[32,33] or ThT[24]) as a way to improve binding affinity to a particular target molecule. To the best of our knowledge, we are the first to combine this with a strategy to enable isolation/precipitation of the target molecule, *i.e.* attach a biotin moiety the polymer linker between ligands.

The CAP-1 structure was successfully designed and then demonstrated to bind and isolate aggregates with amyloid structure (oligomers and fibrils of $a\beta_{42}$, tau and α-synuclein), but crucially not monomers, in model experiments using synthetic aggregates. However, it is also critical to be demonstrate translational relevance. In vivo, the complexity of the biofluids that surround the CNS (CSF) and the brain tissue itself makes the detection of small amyloids a major challenge. We were able to show that the sensitive detection of amyloid containing aggregates can be performed in CSF by amyloid pulldown using CAP-1, followed by bead digestion and detection by mass spectrometry. This new capability for unbiased detection and capture of amyloids, coupled with a mass spectrometry approach to provide the molecular composition is a powerful combination because it has the potential to define the amyloids present in the brain and CSF in biological contexts. Furthermore, we demonstrated that we could capture the aggregates responsible for membrane permeabilisation, present in CSF. Since this sample is enriched in aggregates without monomers being present, this approach allows the further characterization of these human derived aggregates and cytotoxicity experiments to be performed. Further improvements to the design of the capture molecule are possible by optimising the linker length, head groups and synthesising mutlimeric molecules to further improve the sensitivity and selectivity of amyloid precipitation. There may also be significant advantages in this approach in terms of stability and resistance to degradation compared to conventional antibodies.

In conclusion, we have successful developed a new molecule inspired in the trimeric shape of an antibody. CAP-1 has two binding sites improve avidity and a third moiety to enable surface for immobilisation and therefore, capture of aggregates based on their structure not their protein composition. This simple and versatile method requires minimal manipulation and can be used to study protein aggregates present in human biofluids. On-bead digestion and further optimisation will allow identification of molecular components of aggregates using mass spectrometry. Overall, this non-biased approach will pave the way to understanding the exact molecular species responsible for neurodegeneration in humans and consequently hasten development of simple and robust early diagnosis methods.

Acknowledgements

HZ is a Wallenberg Scholar supported by grants from the Swedish Research Council (#2018-02532), the European Research Council (#681712), Swedish State Support for Clinical Research (#ALFGBG-720931) and the UK Dementia Research Institute at UCL. DK is supported by grants from the European Research Council (#669237), the Royal Society and UK Dementia Research Institute at Cambridge. We thanks the Royal Society for the University Research Fellowship os SFL (UF120277).

Conflicts of interest

HZ has served at scientific advisory boards for Roche Diagnostics, Wave, Samumed and CogRx, has given lectures in symposia sponsored by Alzecure and Biogen, and is a co-founder of Brain Biomarker Solutions in Gothenburg AB, a GU Ventures-based platform company at the University of Gothenburg (outside submitted work).

Supplementary Information

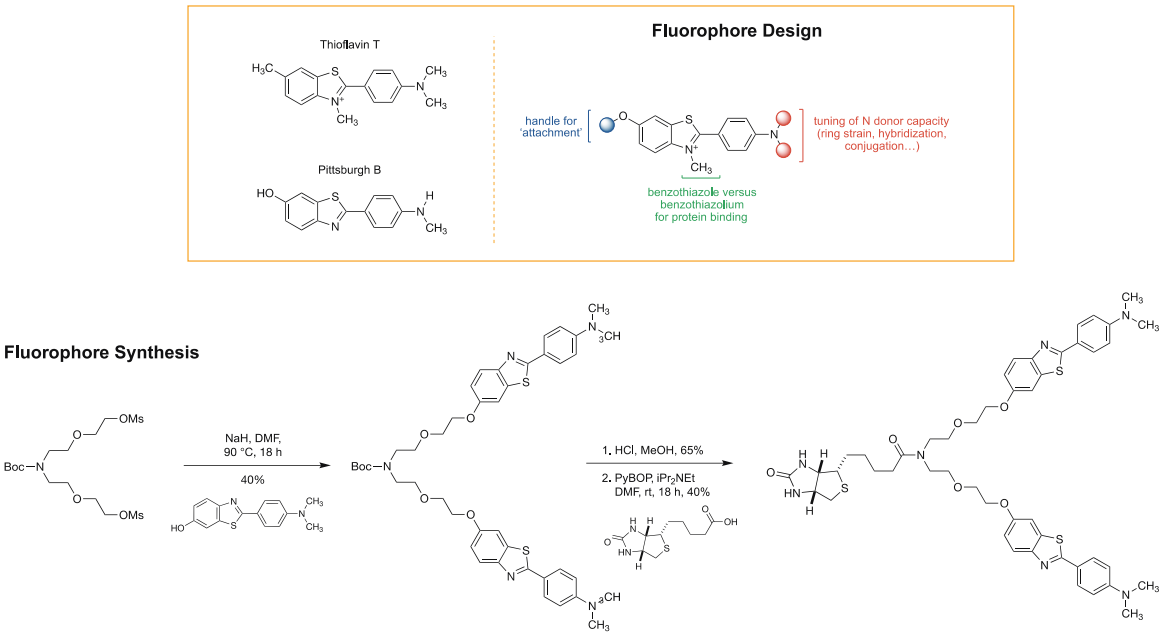

SI.1 - Rational design and characterization of CAP-1. (**a**) Outline of CAP-1design and synthesis.

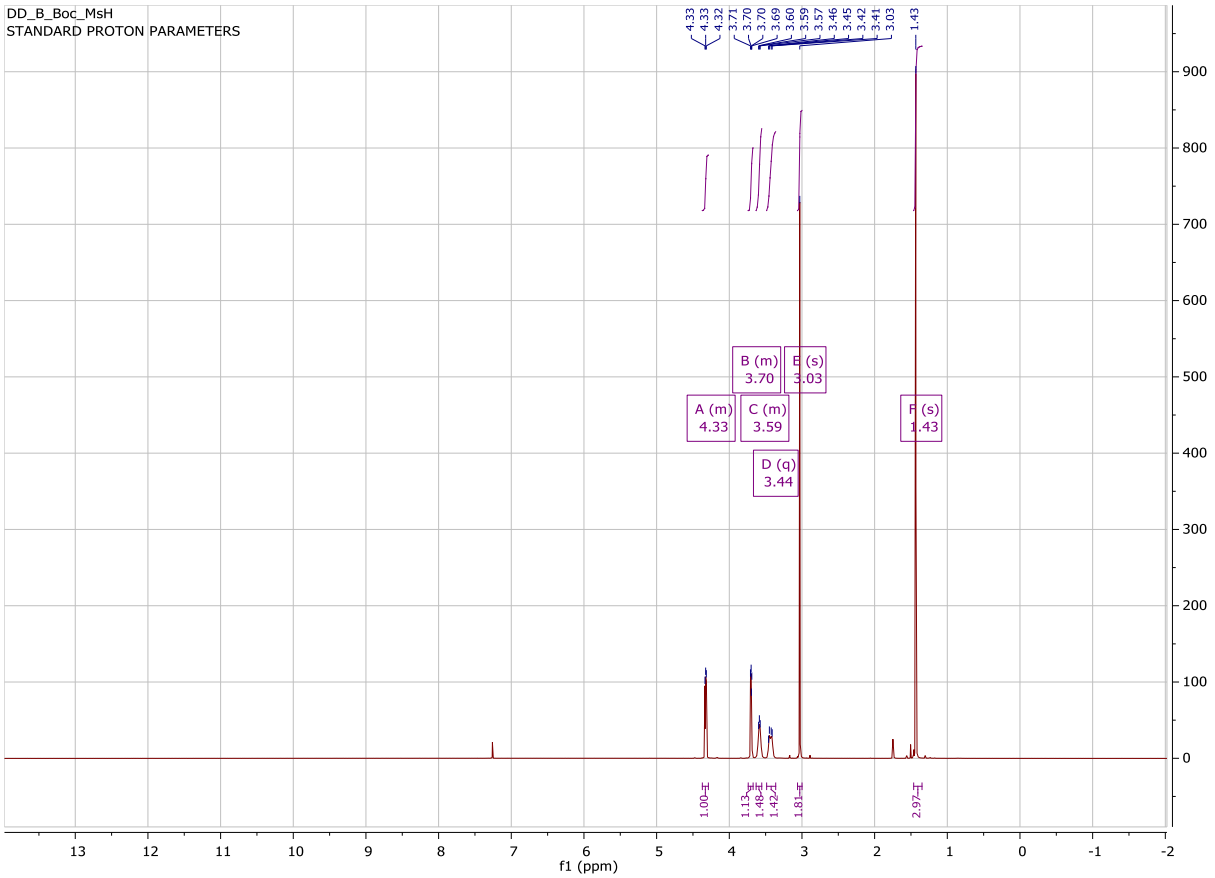

SI.2 - 1H NMR spectra of (**A**) bis-Mesylate.

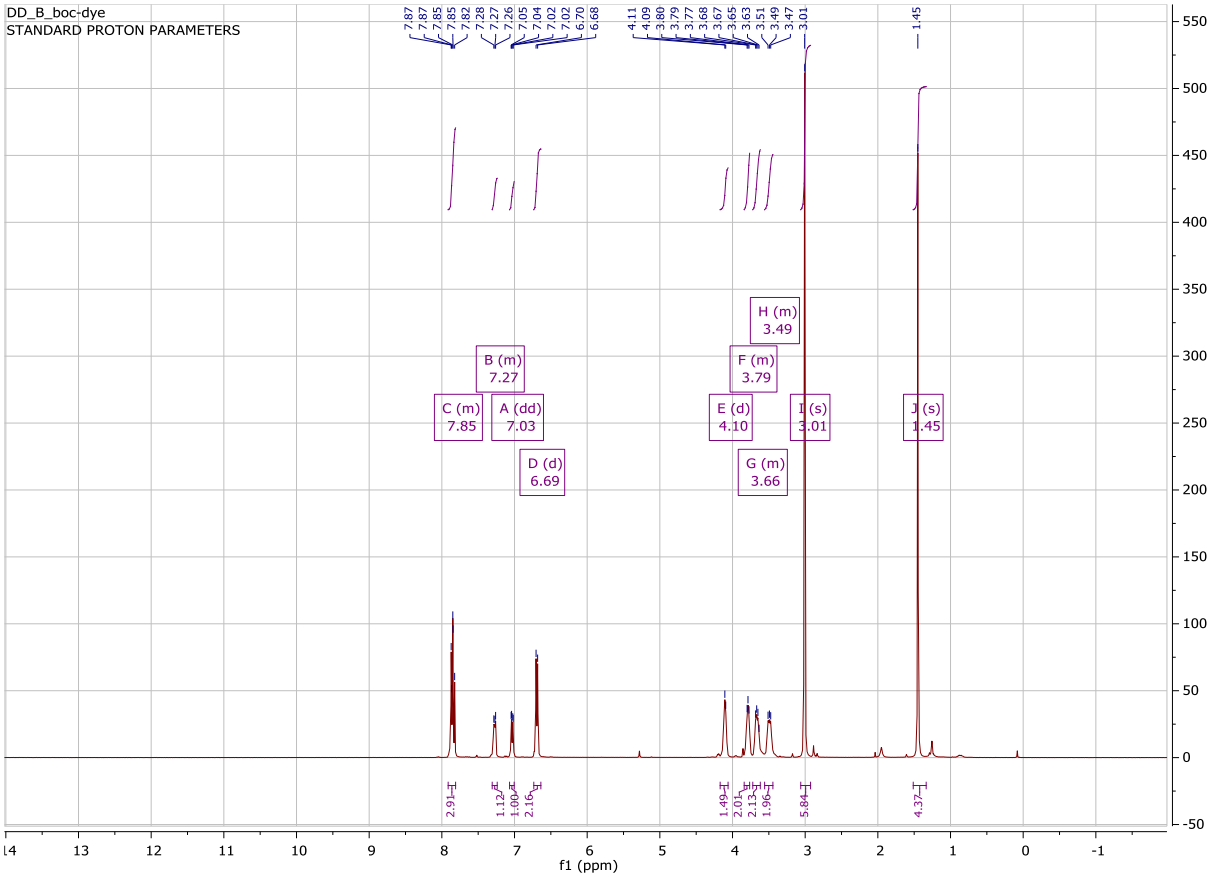

SI.3 - 1H NMR spectra (B) Boc-protected bis-benzothiazole.

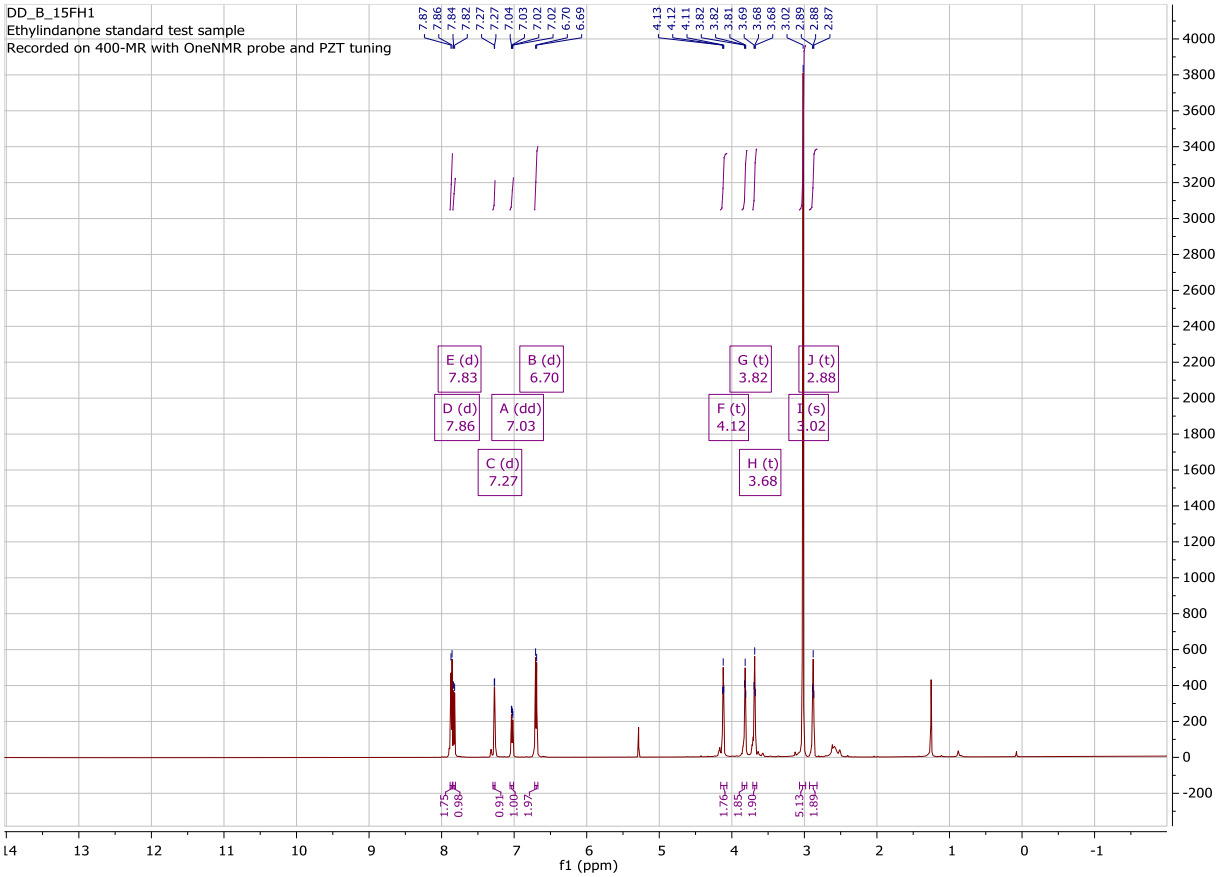

SI.4 - 1H NMR spectra (C) NH bis-benzothiazole.

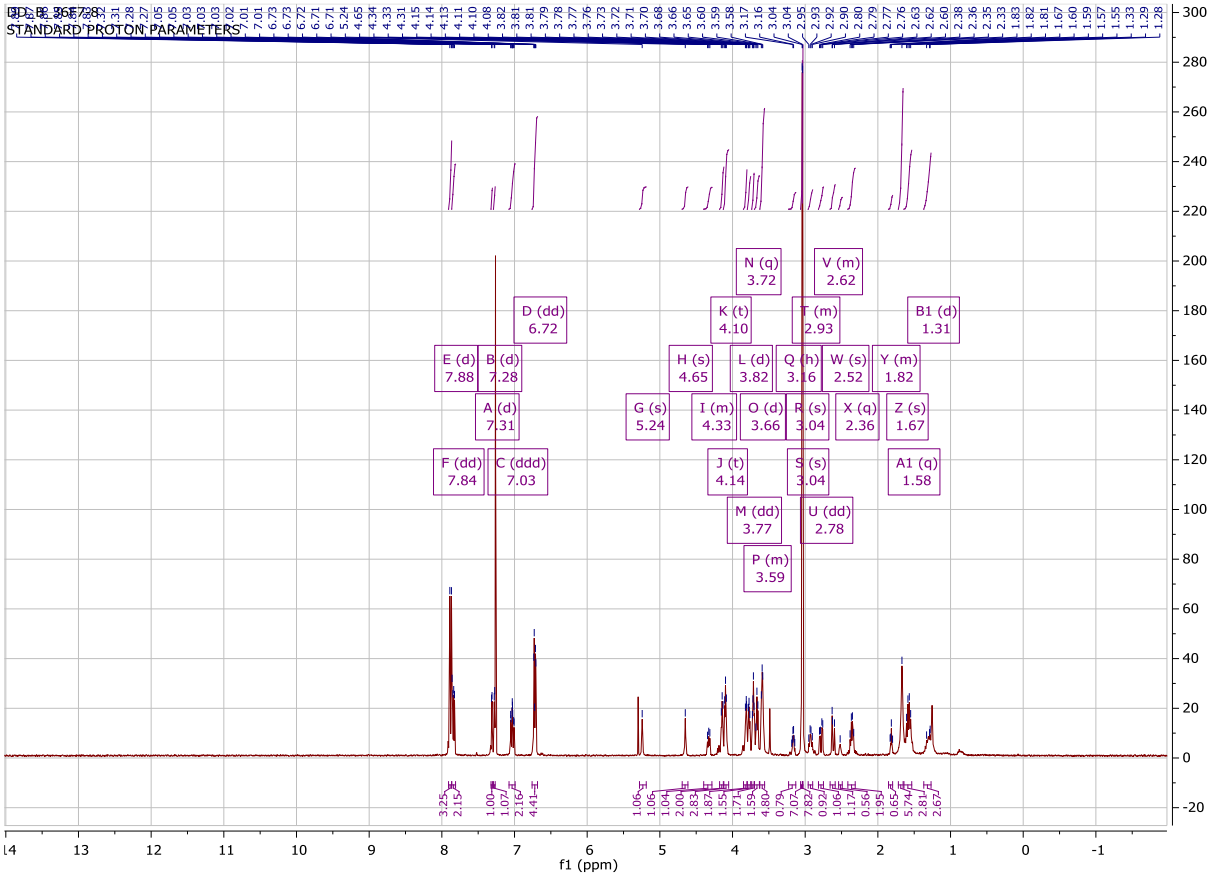

SI.5 - 1H NMR spectra (D) N-Biotinylated bis-benzothiazole.

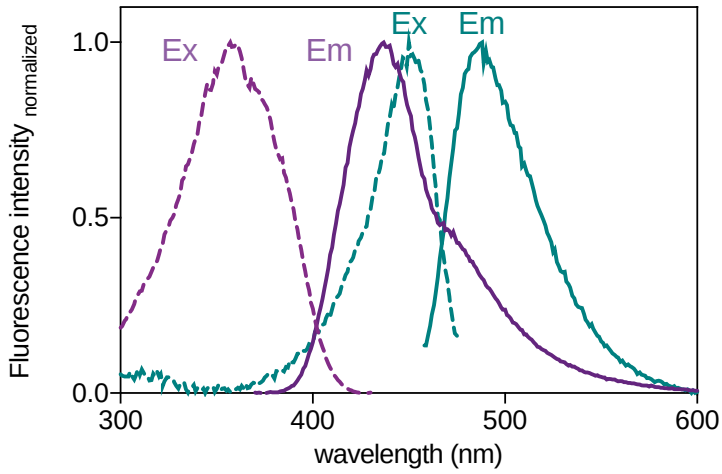

SI.6 - Excitation and emission spectrum of 20 μM CAP-1(-) and 20 μM ThT (-) in the presence of 10 μM α–synuclein fibrils.

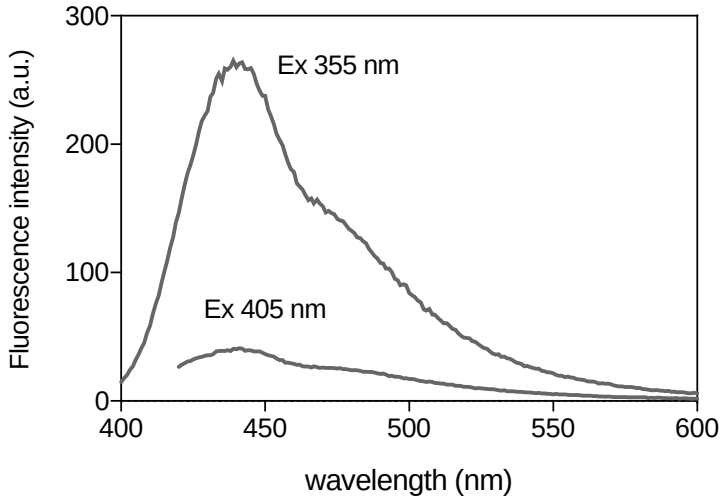

SI.7 - Decrease in the fluoresce intensity of α−synuclein fibrils emission spectrum from using using λ_{ex}=355 nm to λ_{ex}=405 nm.

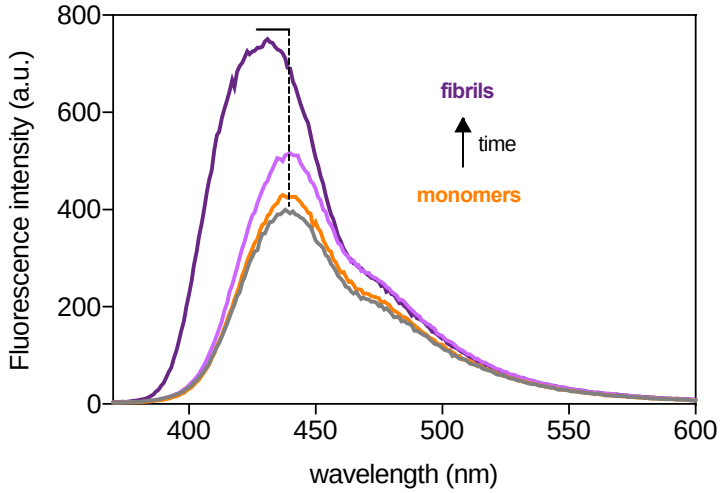

SI.8 - Emission spectra of 20 μM CAP-1 alone and in the presence of different time points of 10 μM α–synuclein aggregation reaction: CAP-1 only (——), t=0h (—— monomers), t=8h (—— oligomers) and t=24h (—— fibrils).

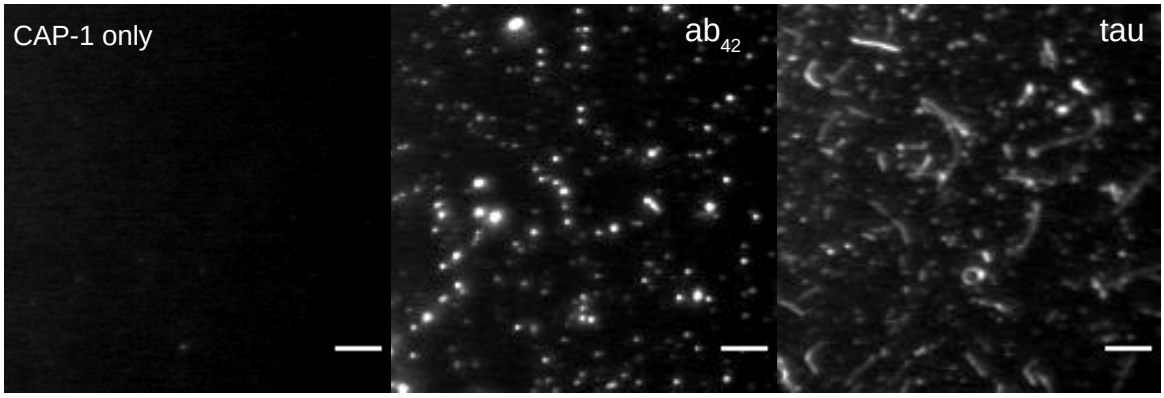

SI.9 - TIRFM images of 5 μM CAP-1 only (left panel), with 1 μM aβ$_{42}$ (middle) and with 100 nM tau (right). Scale bar = 5 μm.

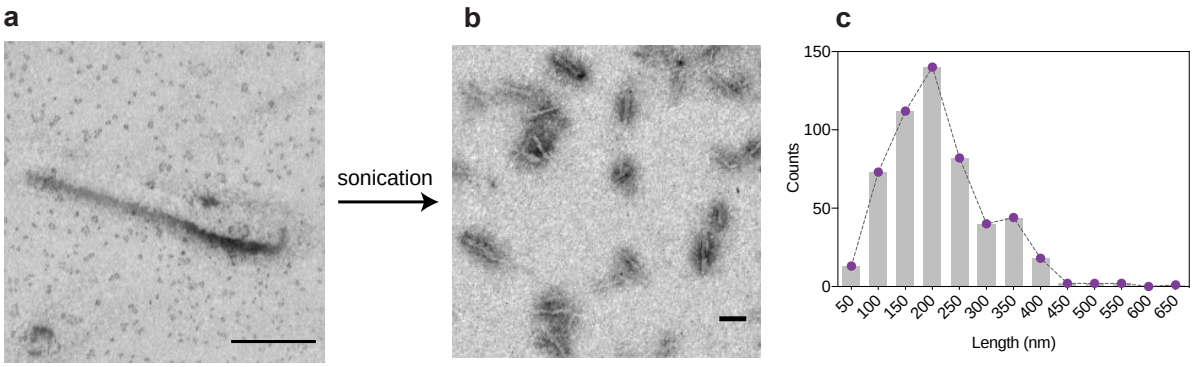

SI.10 - STEM images of α–synuclein fibril before and after sonication. (**a**) fibril length ~3 μm. Scale bar = 1 μm. (**b**) α–synuclein fibrils sonicated, scale bar = 200 nm and (**c**) histogram of fibril length distribution from 549 individual aggregates.

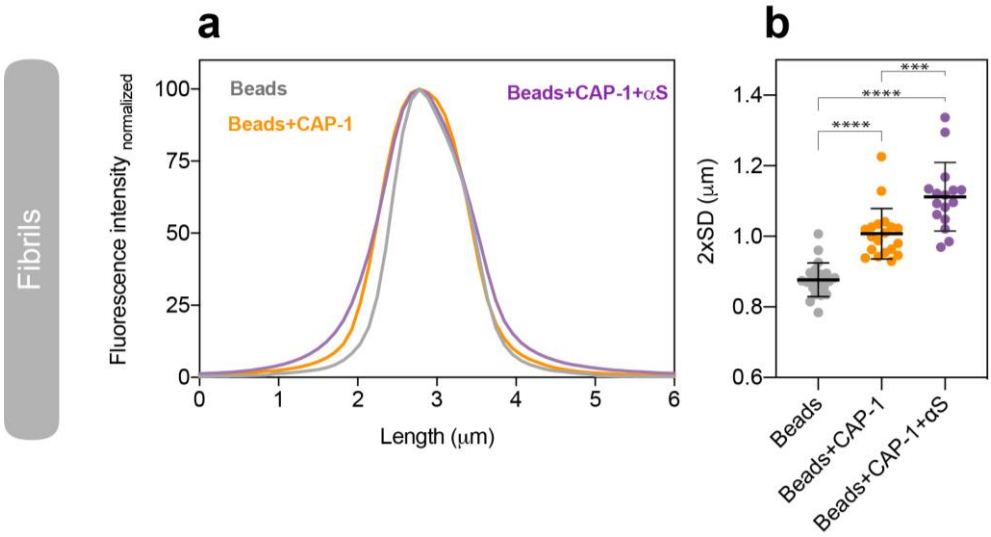

SI.11 - Normalized fluorescence intensity profile of beads. **(a)** Average of intensity profiles for beads alone (—), in the presence of CAP-1 (—) and in the presence of CAP-1 and α-synuclein (—). **(b)** Width of the fluorescence intensity profile measured as the double of the standard deviation (SD) of the Gaussian fitting of the average of all beads' profiles per sample, error bar corresponds to the SEM of the fitting. **(c)** Width of the fluorescence intensity profile measured as the double of the standard deviation (SD) of the Gaussian fitting for each bead profile separately (two independent experiment per sample at least 30 beads measured). Error bar corresponds to the SD of the bead-to-bead variation and the p-value corresponds to the result of a one-way ANOVA, and Tukey's post hoc comparison. **** $p<0.0001$, ***$p=0.0002$.

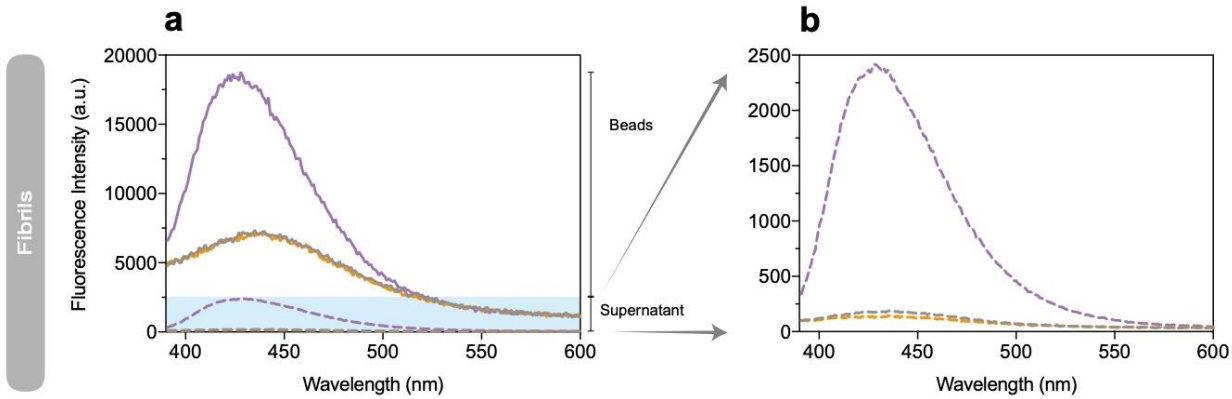

SI.12 - Read-out of protein capture mediated by CAP-1. Emission spectrum of beads and supernatant after AP using 10 μM α−synuclein sonicated fibrils, (**a**) beads and supernatant and (**b**) supernatant.

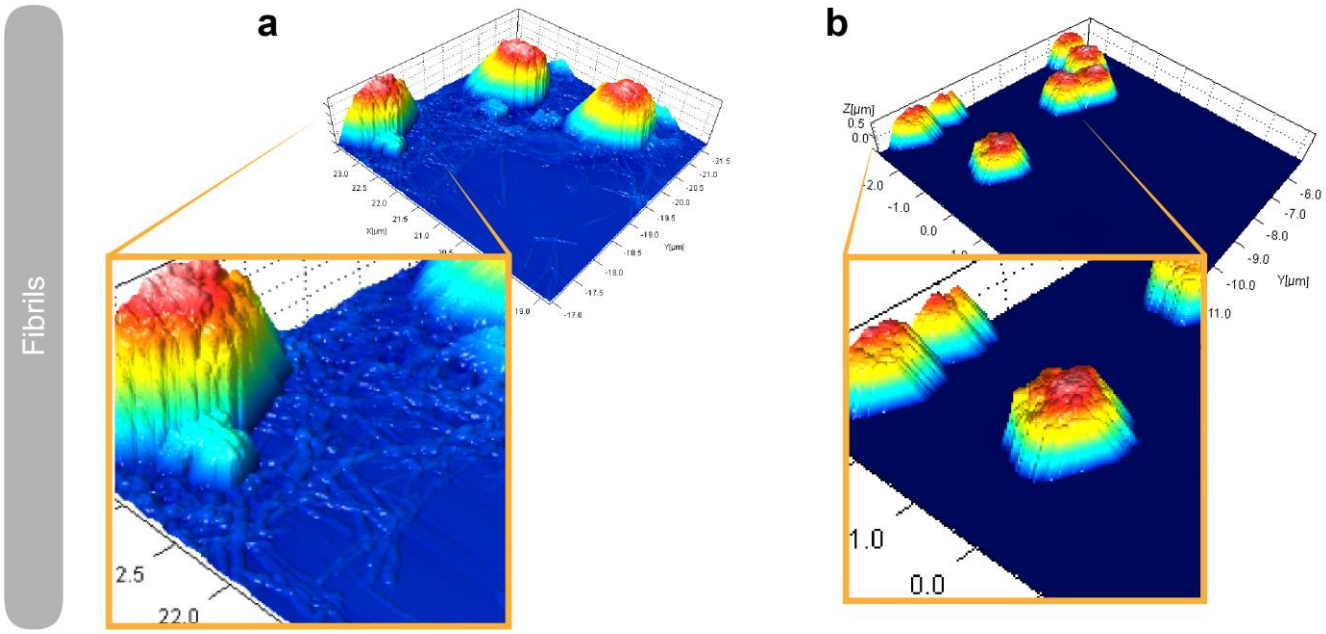

SI.13 - AFM height images after AP in the presence a) and absence b) of α-synuclein fibrils. Fibrils preferentially localize around the beads a).

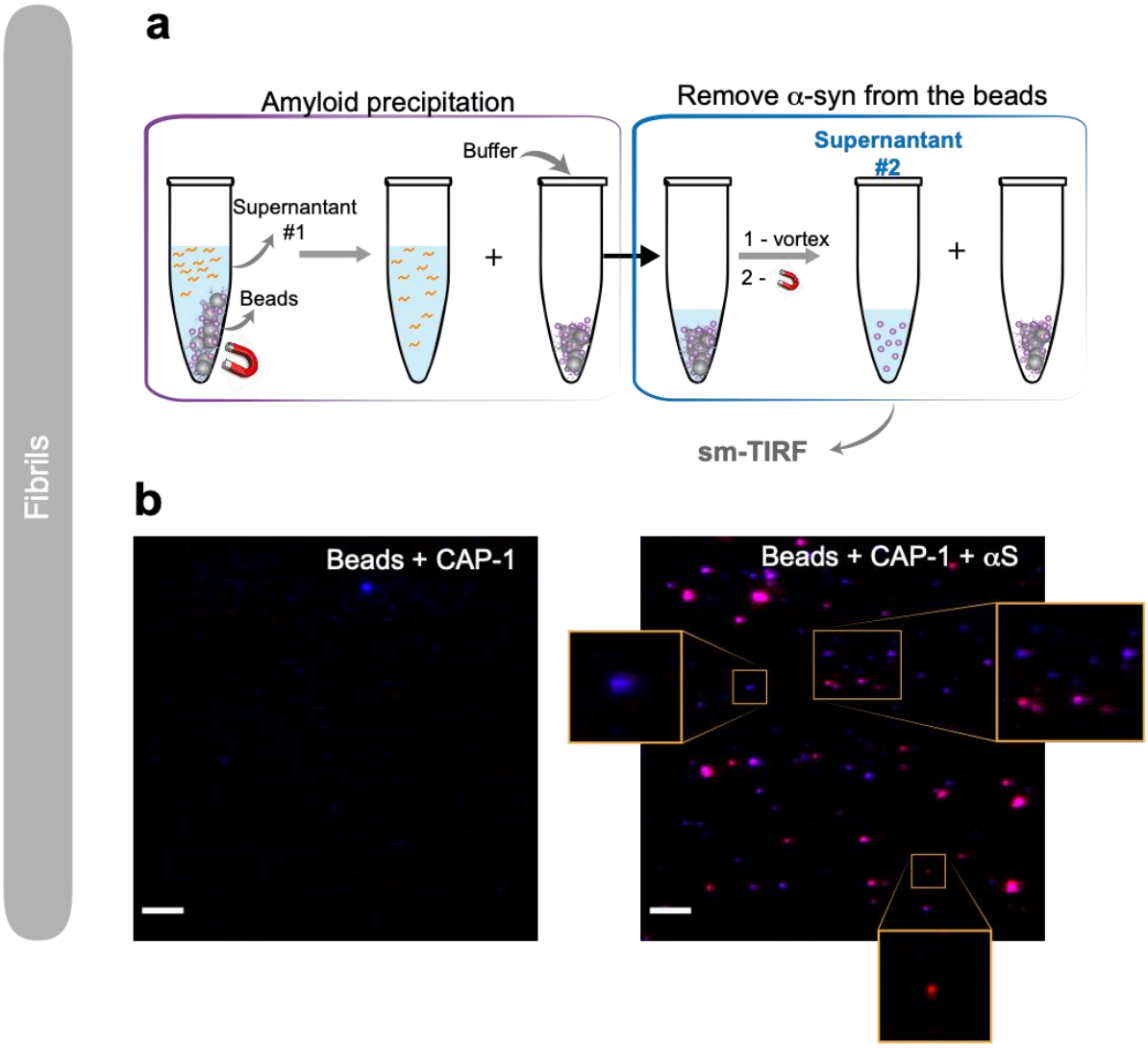

SI.14- Removal of α-synuclein aggregates from beads. **(a)** Outline of the AP protocol followed by a second dilution and incubation of beads with a small volume of buffer and 5 cycles of 30 sec vortex. **(b)** TIRFM of the new supernatant fraction (#2) after addition of 5 μM ThT. Left, beads+CAP-1 (control) and right beads+CAP-1+ α-synuclein. Images are the result of co-localizing CAP-1 (434/17-25 emission filter - red) and ThT (480/40-25 nm emission filter - blue) channels. The presence of aggregates labelled in blue, red or pink is consistent with the successful removal of aggregates from the beads. Given the reduced overlap between the two channels it is possible to conclude that: aggregates labelled in blue were only labelled by ThT (added prior to imaging) and are therefore free of CAP-1; aggregates labelled in red are aggregates that only have CAP-1 from the beads attached to them; and finally the pink aggregates are larger aggregates where despite the presence of CAP-1 from the beads also ThT found available binding sites.

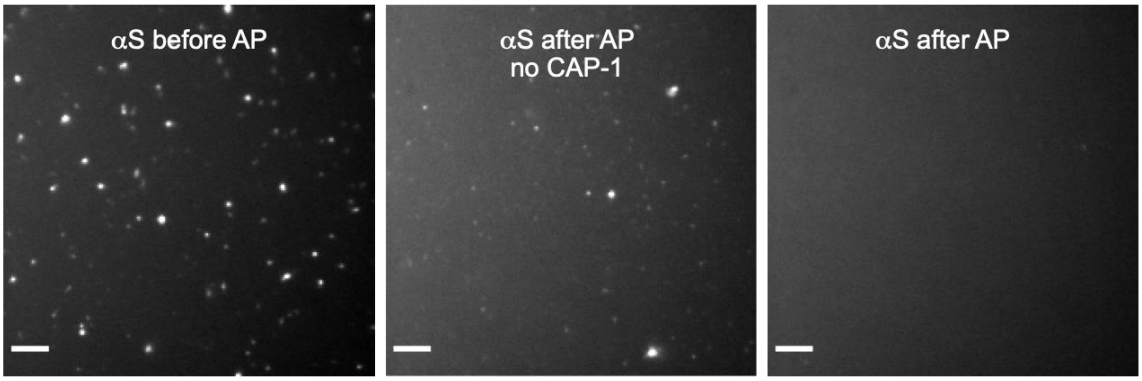

SI.15 – Amyloid-precipitation (AP) of early aggregates using CAP-1. TIRFM 7 μM α-synuclein before (left) and after AP in the presence (right) and absence (middle) of 5 μM CAP-1 using the supernatant fraction. In the middle and right panel, we used 3x times the volume used in the left (before AP) *i.e.* the equivalent to 21 μM to increase the fluorescent puncta signal needed for quantitative analysis. Scale bar = 5 μm.

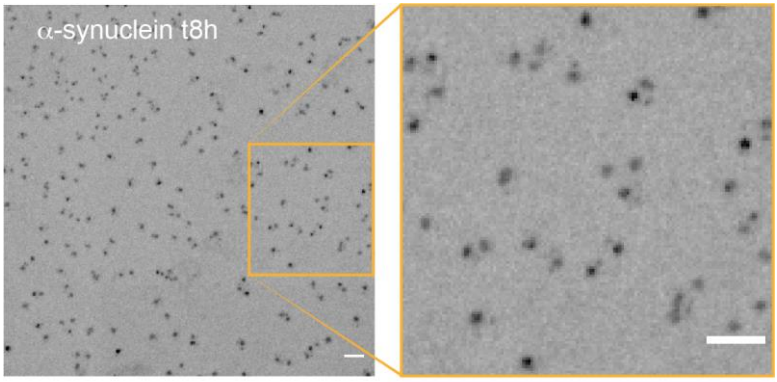

SI.16 - STEM image of α−synuclein oligomers from t=8h in the aggregation reaction (left). Scale bar = 200 nm.

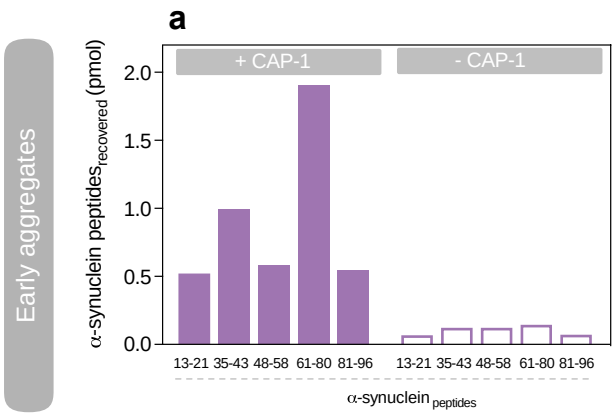

b

Peptide ID	Peptide sequence
α-syn13_21	EGVVAAAEK
α-syn35_43	EGVLYVGSK
α-syn46_58	EGVVHGVATVAEK
α-syn61_80	EQVTNVGGAVVTGVTAVAQK
α-syn81_96	TVEGAGSIAAATGFVK

SI.17 – (a) PRM-MS quantification of α-synuclein peptides recovered after amyloid-precipitation (AP) in presence and absence of CAP-1 using recombinant α-synuclein. **(b)** Table with the amino acid sequence of α-synuclein tryptic peptides used in the experiment.

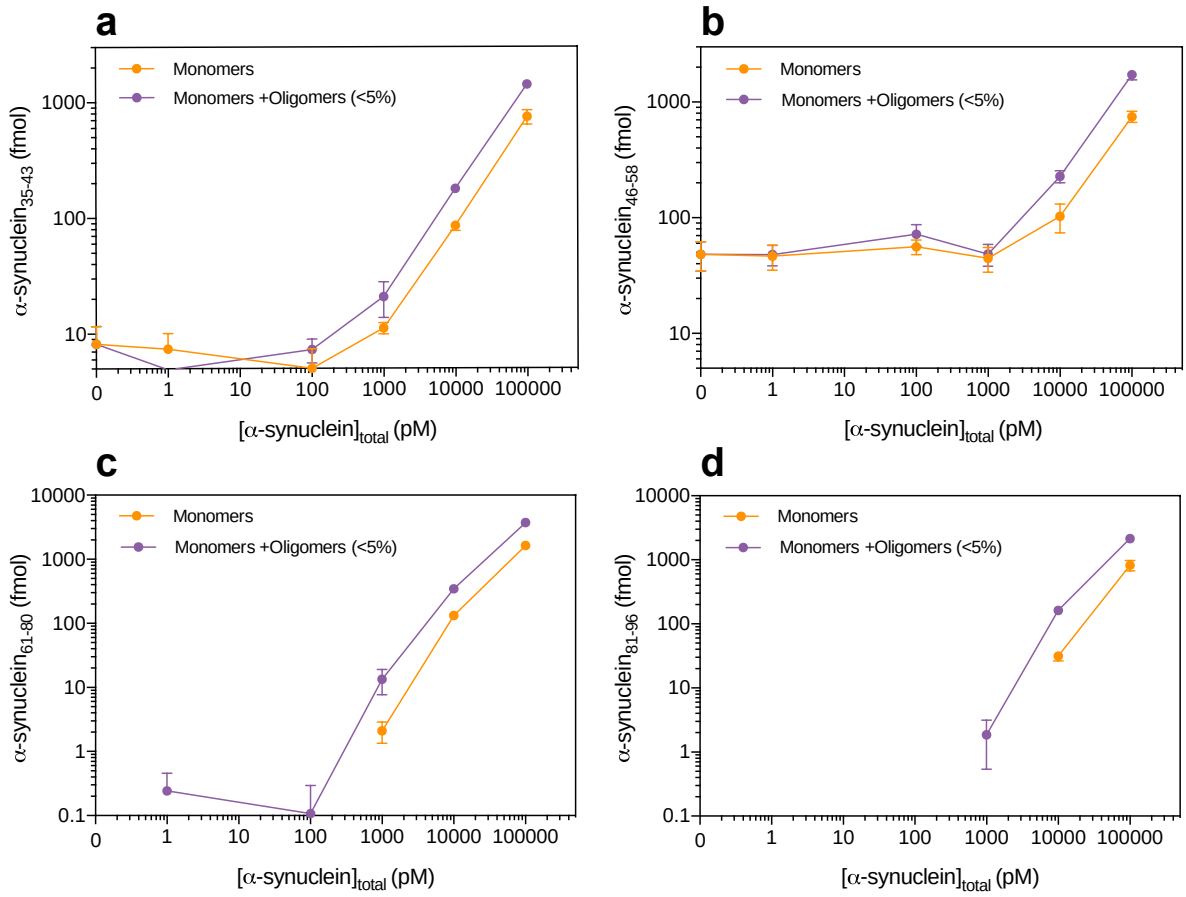

SI.18 - PRM-MS quantification of α-synuclein peptides recovered after amyloid-precipitation (AP) from the background of CSF (complement to Figure 3 of the main text). Prior to AP recombinant α-synuclein (1 pM to 100 nM) monomers or monomers+oligomers were added to control CSF. After AP and on bead digestion the recovered peptides were quantified using PRM-MS **(a)** α-synuclein$_{35-43}$, **(b)** α-synuclein$_{46-58}$, **(c)** α-synuclein$_{61-80}$, **(d)** α-synuclein$_{81-96}$.

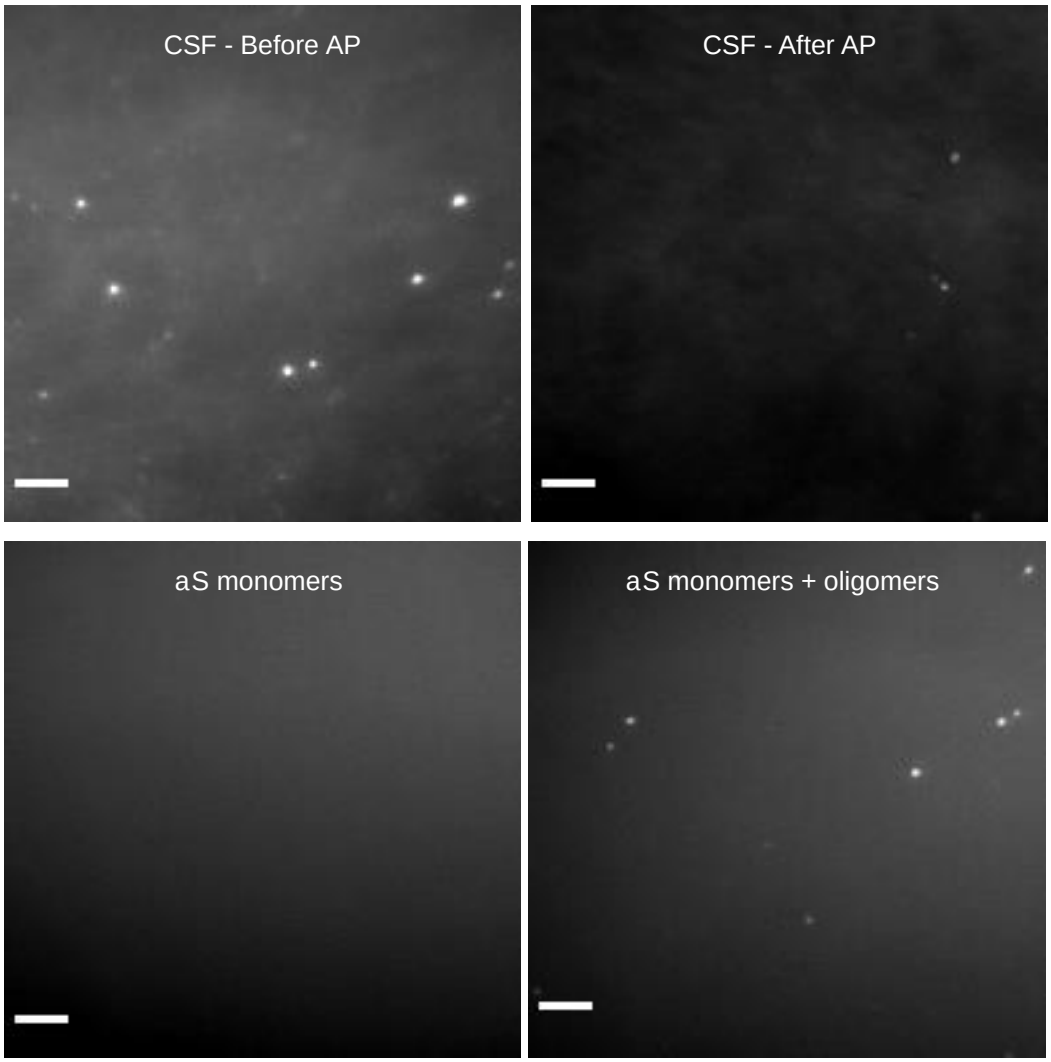

SI.19 – TIRFM images of control CSF and α-synuclein used in Figure 3 of the main text. CSF before and after amyloid - precipitation (top panels, left to right), and α-synuclein monomers and monomers+oligomers (bottom panels, left to right).

References

1. Knowles, T. P. J., Vendruscolo, M. & Dobson, C. M. The amyloid state and its association with protein misfolding diseases. *Nature Reviews Molecular Cell Biology* vol. 15 384–396 (2014).
2. Braak, H. *et al.* Pattern of brain destruction in Parkinson's and Alzheimer's diseases. *J. Neural Transm.* **103**, 455–490 (1996).
3. Lee, J. E. *et al.* Mapping Surface Hydrophobicity of α-Synuclein Oligomers at the Nanoscale. *Nano Lett.* **18**, 7494–7501 (2018).
4. Cremades, N. *et al.* Direct observation of the interconversion of normal and toxic forms of α-synuclein. *Cell* **149**, 1048–1059 (2012).
5. Ludtmann, M. H. R. *et al.* α-synuclein oligomers interact with ATP synthase and open the permeability transition pore in Parkinson's disease. *Nat. Commun.* **9**, 2293 (2018).
6. Whiten, D. R. *et al.* Single-Molecule Characterization of the Interactions between Extracellular Chaperones and Toxic α-Synuclein Oligomers. *CellReports* **23**, 3492–3500 (2018).
7. Mannini, B. *et al.* Stabilization and Characterization of Cytotoxic Aβ 40 Oligomers Isolated from an Aggregation Reaction in the Presence of Zinc Ions. *ACS Chem. Neurosci.* **9**, 2959–2971 (2018).
8. De, S. *et al.* Different soluble aggregates of Aβ42 can give rise to cellular toxicity through different mechanisms. *Nat. Commun.* **10**, (2019).
9. Outeiro, T. F. *et al.* Formation of toxic oligomeric α-synuclein species in living cells. *PLoS One* **3**, 1–9 (2008).
10. Kumar, S. T., Donzelli, S., Chiki, A., Syed, M. M. K. & Lashuel, H. A. A simple, versatile and robust centrifugation-based filtration protocol for the isolation and quantification of α-synuclein monomers, oligomers and fibrils: Towards improving experimental reproducibility in α-synuclein research. *J. Neurochem.* **153**, 103–119 (2020).
11. Iadanza, M. G., Jackson, M. P., Hewitt, E. W., Ranson, N. A. & Radford, S. E. A new era for understanding amyloid structures and disease. *Nat. Rev. Mol. Cell Biol.* **19**, 755–773 (2018).
12. Mitkevich, O. V. *et al.* DNA aptamers detecting generic amyloid epitopes. *Prion* **6**, 400–406 (2012).
13. Rahimi, F. Aptamers selected for recognizing amyloid β-protein—a case for cautious optimism. *Int. J. Mol. Sci.* **19**, 1–20 (2018).
14. Voropai, E. S. *et al.* Spectral properties of thioflavin T and its complexes with amyloid fibrils. *J. Appl. Spectrosc.* **70**, 868–874 (2003).
15. Hoyer, W. *et al.* Dependence of α-synuclein aggregate morphology on solution conditions.

J. Mol. Biol. **322**, 383–393 (2002).

16. Horrocks, M. H. *et al.* Single-Molecule Imaging of Individual Amyloid Protein Aggregates in Human Biofluids. *ACS Chem. Neurosci.* **7**, 399–406 (2016).
17. Bhattacharjee, P. *et al.* Mass Spectrometric Analysis of Lewy Body-Enriched α-Synuclein in Parkinson's Disease. *J. Proteome Res.* **18**, 2109–2120 (2019).
18. Brinkmalm, A., Öhrfelt, A., Bhattacharjee, P. & Zetterberg, H. Detection of α-Synuclein in Biological Samples Using Mass Spectrometry BT - Alpha-Synuclein: Methods and Protocols. in *Alpha-Synuclein: Methods and Protocols* vol. 1948 (Springer New York, 2019).
19. Flagmeier, P. *et al.* Ultrasensitive Measurement of Ca2+ Influx into Lipid Vesicles Induced by Protein Aggregates. *Angew. Chemie - Int. Ed.* **56**, 7750–7754 (2017).
20. Drews, A. *et al.* Inhibiting the Ca2+ Influx Induced by Human CSF. *Cell Rep.* **21**, 3310–3316 (2017).
21. Biancalana, M. & Koide, S. Molecular mechanism of Thioflavin-T binding to amyloid fibrils. *Biochim. Biophys. Acta - Proteins Proteomics* **1804**, 1405–1412 (2010).
22. Klunk, W. E. *et al.* Uncharged thioflavin-T derivatives bind to amyloid-beta protein with high affinity and readily enter the brain. *Life Sci.* **69**, 1471–1484 (2001).
23. Wu, C., Bowers, M. T. & Shea, J.-E. On the Origin of the Stronger Binding of PIB over Thioflavin T to Protofibrils of the Alzheimer Amyloid-β Peptide: A Molecular Dynamics Study. *Biophysj* **100**, 1316–1324 (2011).
24. Qin, L., Vastl, J. & Gao, J. Highly sensitive amyloid detection enabled by thioflavin T dimers. *Mol. Biosyst.* **6**, 1791–1795 (2010).
25. Ye, L. *et al.* In vitro high affinity α-synuclein binding sites for the amyloid imaging agent PIB are not matched by binding to Lewy bodies in postmortem human brain. *J. Neurochem.* **105**, 1428–1437 (2008).
26. Sulatskaya, A. I. *et al.* Investigation of α-synuclein amyloid fibrils using the fluorescent probe thioflavin T. *Int. J. Mol. Sci.* **19**, (2018).
27. De, S. *et al.* Different soluble aggregates of Aβ42 can give rise to cellular toxicity through different mechanisms. *Nat. Commun.* **10**, 1511–1541 (2019).
28. Xiong, F., Ge, W. & Ma, C. Quantitative proteomics reveals distinct composition of amyloid plaques in Alzheimer's disease. *Alzheimer's Dement.* 1–12 (2018).
29. Heywood, W. E. *et al.* Identification of novel CSF biomarkers for neurodegeneration and their validation by a high-throughput multiplexed targeted proteomic assay. *Mol. Neurodegener.* 1–16 (2015).
30. Guldbrandsen, A. *et al.* In-depth characterization of the cerebrospinal fluid (CSF) proteome

displayed through the CSF proteome resource (CSF-PR). *Mol. Cell. Proteomics* **13**, 3152–3163 (2014).

31. Selkoe, D. J. The molecular pathology of Alzheimer's disease. *Neuron* **6**, 487–498 (1991).
32. Kramer, R. H. & Karpen, J. W. Spanning binding sites on allosteric proteins with polymer-linked ligand dimers. *Nature* **395**, 710–713 (1998).
33. Liang, J. *et al.* Dimerization of α-Conotoxins as a Strategy to Enhance the Inhibition of the Human α7 and α9α10 Nicotinic Acetylcholine Receptors. *J. Med. Chem.* **63**, 2974–2985 (2020).